AN ANALYSIS OF X-BAND RADIATION FOR SPACE-BASED WIRELESS POWER TRANSMISSION

THESIS

Noah W. Friz, 1st Lieutenant, USAF

AFIT-ENG-MS-21-M-037

DEPARTMENT OF THE AIR FORCE
AIR UNIVERSITY

AIR FORCE INSTITUTE OF TECHNOLOGY

Wright-Patterson Air Force Base, Ohio

AFIT-ENY-MS-15-M-000

AN ANALYSIS OF X-BAND RADIATION FOR SPACE-BASED WIRELESS POWER TRANSMISSION

THESIS

Presented to the Faculty

Department of Electrical Engineering

Graduate School of Engineering and Management

Air Force Institute of Technology

Air University

Air Education and Training Command

In Partial Fulfillment of the Requirements for the

Degree of Master of Science in Electrical Engineering

Noah W. Friz, BS

1st Lieutenant, USAF

March 2020

AFIT-ENY-MS-15-M-000

AN ANALYSIS OF X-BAND RADIATION FOR SPACE-BASED WIRELESS POWER TRANSMISSION

Noah W. Friz, BS

1st Lieutenant, USAF

Committee Membership:

Dr. Andrew J. Terzuoli
Chair

Dr. Steven T. Fiorino
Member

Dr. Jack E. McCrae
Member

Lt. Col Brian E. Hans
Sponsor

AFIT-ENY-MS-15-M-000

Abstract

The USAF is interested in developing a solar powered satellite power beaming system using X-Band radiation for power beaming purposes. To determine the expected level of transmission efficiency of the system, an atmospheric characterization and radiative transfer modeling system called LEEDR was employed. A study was conducted to validate LEEDR's performance while working with microwave frequencies by attempting to replicate brightness temperatures measured by a 10.7 GHz radiometer above the Pacific Ocean in 1999. The results were inconclusive. The climatology data used to create the 1999 atmosphere at times of radiometer measurement was too coarse to accurately determine the state of the weather. Additionally, the impact microphysical weather parameters have on brightness temperature measurements, namely the size, amount, and location of water particles, is significant. These parameters were not included within the climatology data set, nor climatologies produced with pre-2000 numerical weather prediction models. Their parameters are however vital in properly modeling radiative transfer for microwave frequency radiation. Brightness temperature vs. rain rate curves developed within other studies for X-Band radiation curves could however be replicated within LEEDR, and therefore the associated path transmission and extinction values. These values can then serve as a lookup table between brightness temperatures and attenuation for 10 GHz radiation, which provide a useful metric for determining expected transmission efficiencies.

Acknowledgments

I would like to express my appreciation to each member of my thesis committee: Dr. Andrew Terzuoli, Dr. Jack McCrae, Dr. Steven Fiorino, and Lt. Col Brian Hans. Thank you for your support, counsel, and expertise in the development of this research. Each of you has been a true pleasure to work with and know. It is my sincerest hope that our work together serves as a useful foundation in the development of a life-long dream – a wireless world.

A special thanks goes out to Ms. Jaclyn Schmidt, and Mr. Brannon Elmore for answering my dozens of questions about LEEDR, helping me find useful data sets, and debugging many lines of code.

And most importantly, I thank the King of kings for the amazing series of unlikely coincidences that brought me to this project, and such wonderful people. All that I do, I do for You.

Noah W. Friz

Table of Contents

Page

List of Figures

Page

List of Tables

Page

AN ANALYSIS OF X-BAND RADIATION FOR SPACE-BASED WIRELESS POWER TRANSMISSION

I. Introduction

General Issue

Millions of terawatts of sunlight pass through the region of space surrounding Earth in which satellites orbit daily. A fraction of this power would be enough to satisfy energy needs for military operations, if it could be harnessed and transported in a usable form.

In the 1960s, Peter Glaser, detailed a novel approach to global energy: the Solar Power Satellite (SPS). The concept of the original SPS is a large platform positioned in space which continuously collects and converts solar energy into electricity. This power is then used to drive a power beaming system that sends the collected energy to receivers on Earth. This would offer implementations unaffected by nighttime, weather, and seasonal variation. Space solar power could enable global power distribution without a global grid infrastructure, overcoming critical limitations of ground-based solar power systems. For forward operating bases (FOBs), space solar power could reduce considerable logistical burdens and dangers associated with transporting fuel to its destination.

A solar power satellite system needs to accomplish two functions: collection of energy and delivery of that energy to the point of need. The ensemble that performs these functions can be divided into two major segments: the space segment and the Earth segment [18].

This thesis focuses on the power beaming method through the Earth segment and will cover the viability of using X-Band radiation for the wireless transmission of power through the atmosphere. This research seeks to develop long term attenuation statistics that will provide insight on the suitability of an X-Band (8-12 GHz) Solar Power Satellite for power beaming purposes.

Problem Statement

The Air Force Research Laboratory (AFRL) has come to AFIT with a design for a 10 GHz SPS project. AFRL is interested in characterizing the initial design's expected performance.

To characterize the proposed design, one can start by looking at the biggest hurdle a power beaming system faces: the Earth's atmosphere. As an electromagnetic signal propagates through the atmosphere, there is a reduction in intensity caused by the interaction between the signal and atmospheric gases. In general, scattering and absorption account for this attenuation.

Uncondensed water vapor and oxygen can be strongly absorptive of radio signals. This is due to the existence of absorption lines in the elements composing atmospheric gases, or bands of frequencies where these gases naturally absorb photon energy. This occurs at the resonant frequencies of the molecules themselves. An example of the attenuation of water and oxygen, as a function of frequency, is shown in the figure below [26].

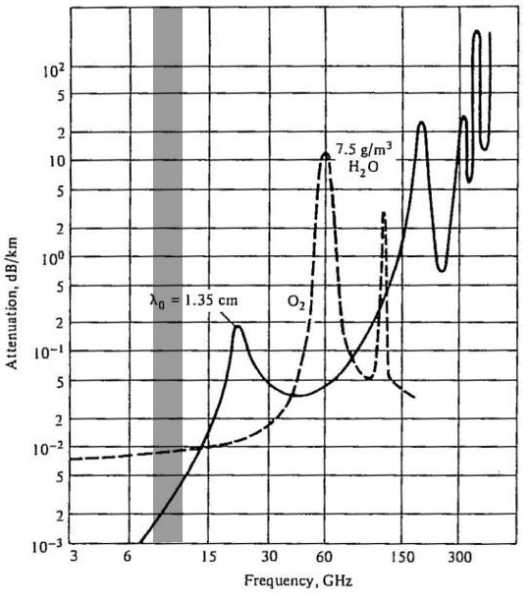

Figure 1. Atmospheric Attenuation vs. Frequency, X-Band Highlighted In Gray [13]

Table 1 – LEEDR Generated Comparison of Atmospheric Effects on EM Attenuation [20]

Parameter	One-Way Loss (dB/km) 10 GHz	35 GHz	94 GHz
Standard Atmosphere	0.012	0.099	0.383
Rain (mm/hr)			
5	0.089	1.489	5.186
25	0.591	6.943	15.863
75	2.145	18.420	32.891
Clean Continental Cumulus	0.027	0.281	1.387
Fog	0.014	0.126	0.532

By extension, atmospheric attenuation levels are also dependent on the weather, particularly rainfall rates, as shown in Table 1 [20]. Fortunately, the attenuation rates for X-Band radiation are on the order of 1e-2 dB/km.

To properly model X-Band atmospheric attenuation, and thus develop long term attenuation statistics, a sophisticated modeling software is necessary that can both model the signal source and the medium it travels through. AFIT Center of Directed Energy (CDE) developed a directed energy weapon (DEW) simulation package, called the High Energy Laser End-to-End Operational Simulation (HELEEOS), which included a correlated, probabilistic climatological database to assess HEL system performance for realistic atmospheres. A separate model, called the Laser Environmental Effects Definition and Reference (LEEDR), was also developed that allows the export of the first principles atmospheric characterizations for other DEW simulation codes.

LEEDR is a first principles, worldwide, surface-to-100 km, atmospheric characterization and radiative transfer code with spectral range considerations between ultraviolet and radio frequency wavelengths (200 nm to 8.6 m). The two primary goals of LEEDR are (1) create correlated physically realizable vertical profiles of meteorological data and environmental effects, such as gaseous and particle extinction, optical turbulence, and cloud-free line-of-sight (CFLOS), and (2) to allow graphical access to and export of the probabilistic data from the Extreme and Percentile Environmental Reference Tables (ExPERT) database. Vertical profiles generally consist of temperature, water vapor content, pressure, optical turbulence, and extinction effects due to atmospheric particulates and hydrometers at various wavelengths. LEEDR contains detailed databases and characterization algorithms for worldwide climatological data, temporally and spatially varying boundary layer definitions, particulate and molecular data, and allows users to input observed surface conditions. Internally consistent line-by-line and correlated-k distribution radiative transfer algorithms capable of assessing path transmittance, path radiance, and celestial contributions to an observed signal level in true three-dimensional geometry on a spherical earth with any relationship between the target and observer have been incorporated into LEEDR calculations. These capabilities make LEEDR an excellent choice for modeling a variety of weather scenarios an SPS would be likely to face, however it requires validation for RF frequencies, and this validation will be a key focus of this research.

HELEEOS accounts for first principles of radiative transfer, therefore potential exists for HELEEOS to be an improvement over existing modeling methods. Despite this, future research will need to address any potential discrepancies that are brought up when

switching from a laser propagation to an RF propagation simulation. By using HELEEOS to model X-band antenna arrays and the power beam it produces, the capability to provide a full picture of the three-dimensional beam pattern can be generated in order to predict beam propagation in various real-time weather and atmospheric scenarios. Examining turbulence effects on the beam, refractive bending, multiple scattering, and attenuation correlation to experimentally measured strengths are all research areas that HELEEOS can interrogate. By providing first principle physical analysis, HELEEOS gives promise to providing information that can be used to evaluate the power beam. [1]

Research Objectives

The objectives of this research are to first determine the validity of LEEDR generated simulations for attenuation calculations. Then secondly, use LEEDR to develop long-term attenuation statistics for X-Band radiation from space to ground, such that AFRL can ascertain a rough idea for the performance of their proposed SPS design.

Additionally, this research will look into the practicality of adaptive optics for increased transmission efficiency.

Assumptions/Limitations

The proposed SPS transmitter is still under development, and subject to change. Therefore, the exact beam pattern will not be simulated, and instead a simplistic line shaped beam will be used for attenuation characterization within LEEDR.

It is assumed for validation purposes that the Earth's atmosphere from 1999-2020 does not differ significantly.

II. Literature Review

Chapter Overview

The purpose of this chapter is to provide a background on electromagnetic wave propagation theory, radiative transfer theory, an understanding of LEEDR and HELEEOS, the way LEEDR will be validated, the effects of weather phenomenon on X-Band radiation, and the applicability of adaptive optics.

2.1 EM Wave Propagation Theory

Power beaming through the atmosphere requires a solid understanding of the radiative transfer of energy, and the roles the medium plays in it. When sending energy through Earth's atmosphere, the presence of various particles, cause a myriad of effects, including energy scattering, absorbing, refracting.

Index of Refraction:

In a vacuum, the speed of light is defined by the Equation 1:

$$c \equiv \frac{1}{\sqrt{\varepsilon_0 \mu_0}} \qquad (1)$$

Where $\varepsilon_0 = 8.854$ x 10^-12 F/m is the permittivity of free space and μ_0 = 1.257 x 10^-6 N/A^2is the permeability of free space.

For propagation in a medium, the expression for the wave propagation direction vector $\vec{k}$ becomes:

$$|\vec{k}| + i|\vec{k}| = \omega\sqrt{\frac{\varepsilon\mu}{\varepsilon_0\mu_0}}\sqrt{\varepsilon_0\mu_0} = \frac{\omega N}{c} \qquad (2)$$

Where ω is the angular frequency of the wave, N is the complex index of refraction defined by $N = \frac{c}{c'}$ where c' is the approximate phase speed of the wave through the medium (assuming the medium is non-absorbing). N is a complex number and the real part of N defines the phase velocity whereas the imaginary part represents attenuation of the wave. The magnitude of N is generally greater than 1, which implies the wave slows down through the medium. It is important to remember that N is heavily dependent not only upon the medium, but also the frequency of the wave [20].

Scattering

In addition to changes in the phase velocity and attenuation due to medium refraction, incoming radiation can also be scattered off the intended propagation path, as seen in Figure 2. As a result, scattering stands to reduce the total power beamed through medium from a transmitter, to a receiver. The likelihood of scattering however, is dependent upon the size and number of scatterers in the medium as well as the wavelength of the radiation.

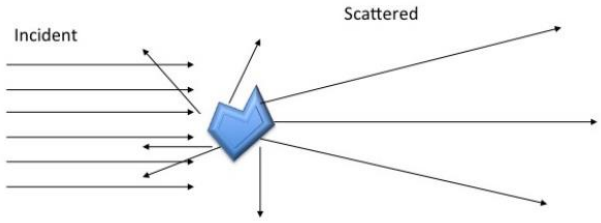

Figure 2. Single Scattering of Incident Wave by Particle [20]

Sensors can't differentiate between absorbed or scattered energy; therefore an extinction coefficient will be defined as the sum of energy absorbed or scattered out of line-of-sight.

$$\beta_e = \beta_s + \beta_a \qquad (3)$$

In order to characterize the extinction as absorption or scattering, the term single scatter albedo, $\tilde{\omega}$ is defined as

$$\tilde{\omega} = \frac{\beta_s}{\beta_e} = \frac{\beta_s}{\beta_s + \beta_a} \qquad (4)$$

$\tilde{\omega}$ has a range of zero in purely absorbing medium, and one in purely scattering medium.

Because scattering of light depends on the wavelength of the incident radiation in relation to the size of the scatterer, it's convenient to describe scattering behavior as a dimensionless size parameter, χ.

$$\chi \equiv \frac{2\pi r}{\lambda} \qquad (5)$$

Where r is the radius of the scattering particle. Figure 3 shows various types of scattering as defined according to their size parameter; note the X-Band regime has been shaded. For wavelengths on the centimeter scale, as with X-Band radiation, it is typical to only address Rayleigh and Mie scattering, ignoring geometric optics. Because this research focuses on wavelengths on the order of a centimeter, we see that scattering will become an issue once scatterer radii equal 10 μm or greater. This corresponds to Rayleigh Scattering for cloud droplets, and drizzle. Raindrops act as Mie Scatterers.

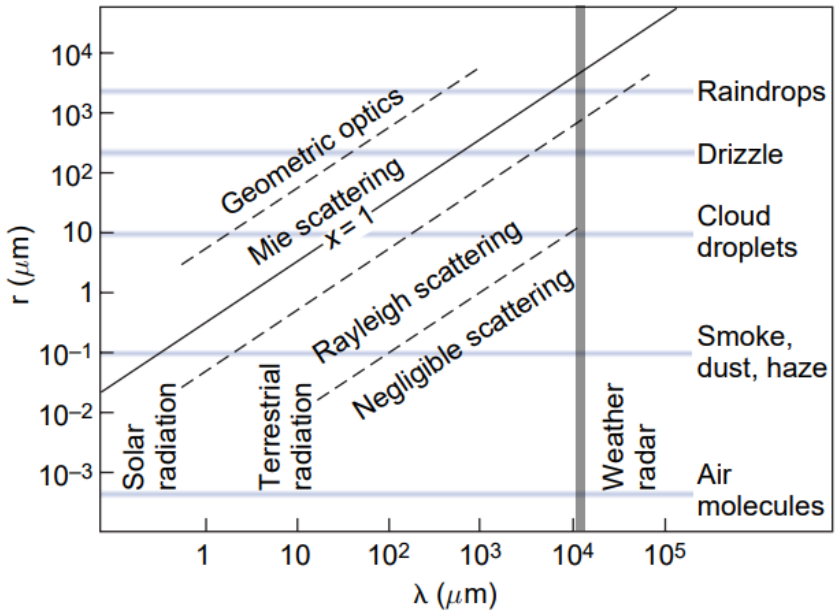

Figure 3. Comparison of Size of Scatterer vs. Wavelength and the various scattering regimes. The shaded box represents the CMW regime. (Modified from Atmospheric Science, 2nd edition, Figure 4.11, pg. 123)

The difference between Rayleigh and Mie Scattering is shown in Figure 4, below. For Mie Scattering, photons are scattered primarily in the forward direction and the larger the particle, the greater forward scattering of energy. Note that the phase function (where the energy is likely to scatter with respect to incident angle) denotes a relatively isotropic distribution for Rayleigh Scattering whereas Mie Scattering is characterized by mostly forward scattering.

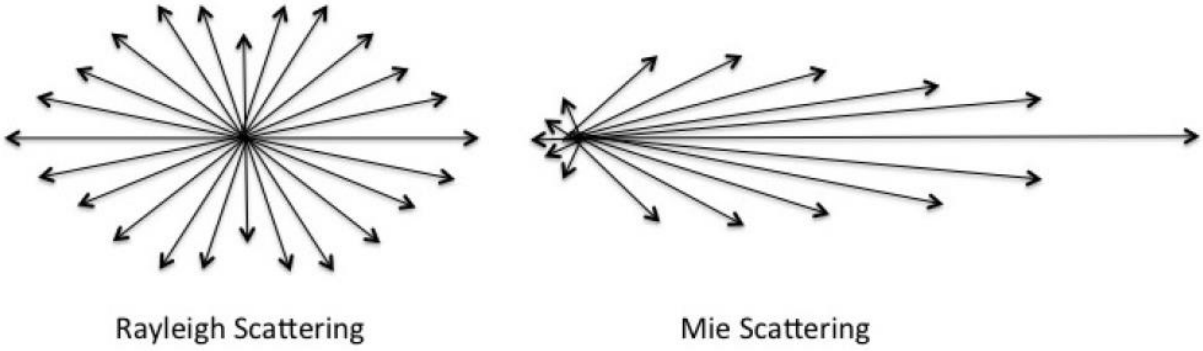

Figure 4. Comparison of Rayleigh and Mie Scattering. For Mie Scattering, larger particles create a more forward pointing scattering pattern [20]

Scattering is important to model as it helps develop a 3-D picture of the radiation pattern as it propagates. Additionally, the various side lobes in an antenna array transmitter will cause complex patterns to develop when scattering takes effect.

Multipath Propagation

The phenomenon of multipath propagation occurs when radiation scatters several times after the initial incidence with the scatterer. With multipath propagation, it is possible for a photon to scatter out of line of sight, and then back into line of sight. This is typically very computationally demanding.

Due to the nature of power beaming, the propagated radiation has a narrow beamwidth, unlike satellite or radio communication signals. As a result, multipath propagation, and its influences can be considered negligible.

Side Lobe Interference

Radiation source beam patterns typically consist of a main beam, and side lobes. An example can be seen in Figure 5. In some cases, side lobe radiation can travel along a path, get reflected, or refracted and then cause interference with the main beam, and thus reducing transmittance. However, for a SPS transmitting to a receiver on the ground, the side lobes are highly likely to travel off to infinity, as there is little in space to redirect their paths, and as a result are of no concern for power beaming purposes.

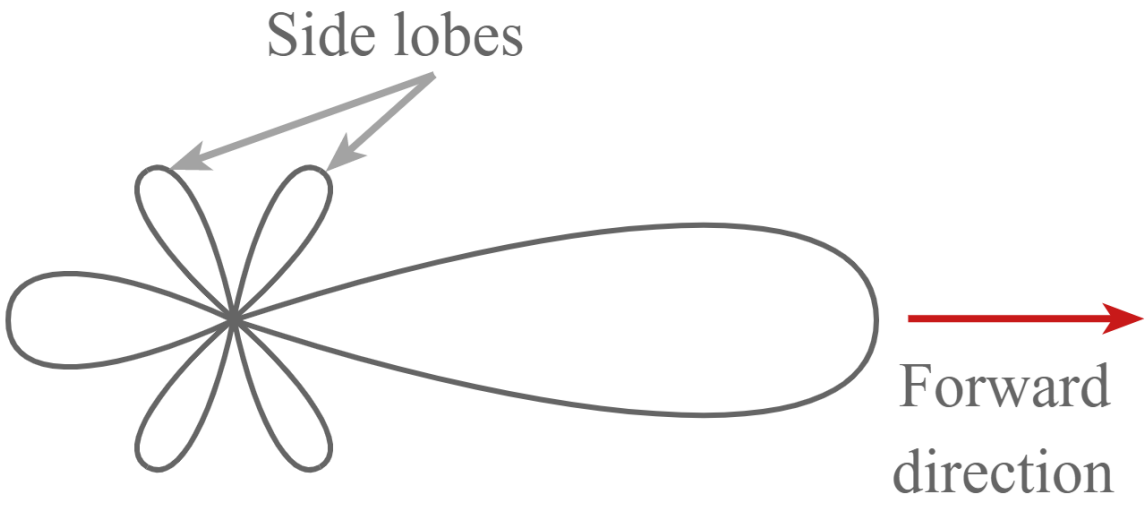

Figure 5. Generic Antenna Beam Pattern

Absorption

Signals propagating through a medium also must account for energy absorption, which further reduces transmitted power. This dynamic can be modeled by a restatement of Beer's Law given in Equation 6 [9]. This law governs the attenuation of photons as they pass through absorbing or scattering medium.

$$F = F_a e^{-\beta_a x} \qquad (6)$$

Where F_a is the incident flux of photons on a parcel of air and F is the flux that makes it through a portion of linear distance x. β_a is the absorption coefficient (in units of inverse length) derived from the imaginary component of N by referencing Equation 2.

$$\frac{\omega}{c} Im\{N\} = \frac{\omega n_i}{c} = \frac{2\pi v n_i}{c} \qquad (7)$$

Where n_i is the magnitude of Im{N} and v is the frequency of the wave in Hertz. Therefore β_a becomes:

$$\beta_a = \frac{4\pi v n_i}{c} = \frac{4\pi n_i}{\lambda} \qquad (8)$$

By referencing Equation 6, one can note that the distance β_a^{-1} is the distance for the wave's propagation to be attenuated by a factor of $\frac{1}{e}$. Note that n_i depends on the permittivity and permeability of the propagation of the medium which is influenced by several parameters such as the size and density of the absorbers. One can also note Equation 8 shows an inverse wavelength dependence on the absorption coefficient.

β_a is dependent on numerous factors, so in order to calculate gaseous absorption, each atmospheric component has been categorized for its effect at specific wavelengths into tabulated databases, HITRAN being among the most notable. HITRAN lists various atmospheric atoms and molecules and the strength of their absorption coefficient in 1/cm. Radiative transfer models take these coefficients and discretize the atmosphere and sum the effects of each atmospheric layer and constituent to get a total path transmittance. This same methodology will apply to X-Band antenna array propagation; by determining the absorbing constituents, a radiative transfer model can determine the strength of the power beam after passing through a parcel of air.

Atmospheric Transmittance Calculations

To determine the change in intensity of an EM wave, one can look to the general form of Beer's Law:

$$I_\lambda = I_{\lambda 0} \exp\left[-\int_{s1}^{s2} \beta_e(s) ds\right] \qquad (9)$$

Equation 9 calculates the final intensity of the incident EM radiation after passing through a homogenous parcel of air with an extinction cross section β_e where the path is defined by s1 and s2.

The value of the integral in Equation 9 is defined as the optical path (τ) which is analogous to optical depth/thickness when measured vertically.

$$\tau \equiv \int_{s1}^{s2} \beta_e(s) ds \qquad (10)$$

When taking the exponent of Equation 10, the transmittance is calculated over a path s:

$$t \equiv e^{-\tau} \qquad (11)$$

Transmittance is a number from zero to one where zero is an opaque atmosphere, and 1 is a transparent atmosphere. When discretizing the atmosphere into layers, the total transmittance is the product of each layer's transmittance. The total optical depth is the sum of all optical depths [9].

Absorption in the X-Band Regime

In the X-Band regime (8-12 GHz), molecular absorption is mainly due to water and oxygen. Figure 6 depicts their specific attenuations as a function of frequency. It can be noted that specific attenuation of their combined absorption levels is on the order of 0.01 dB/km.

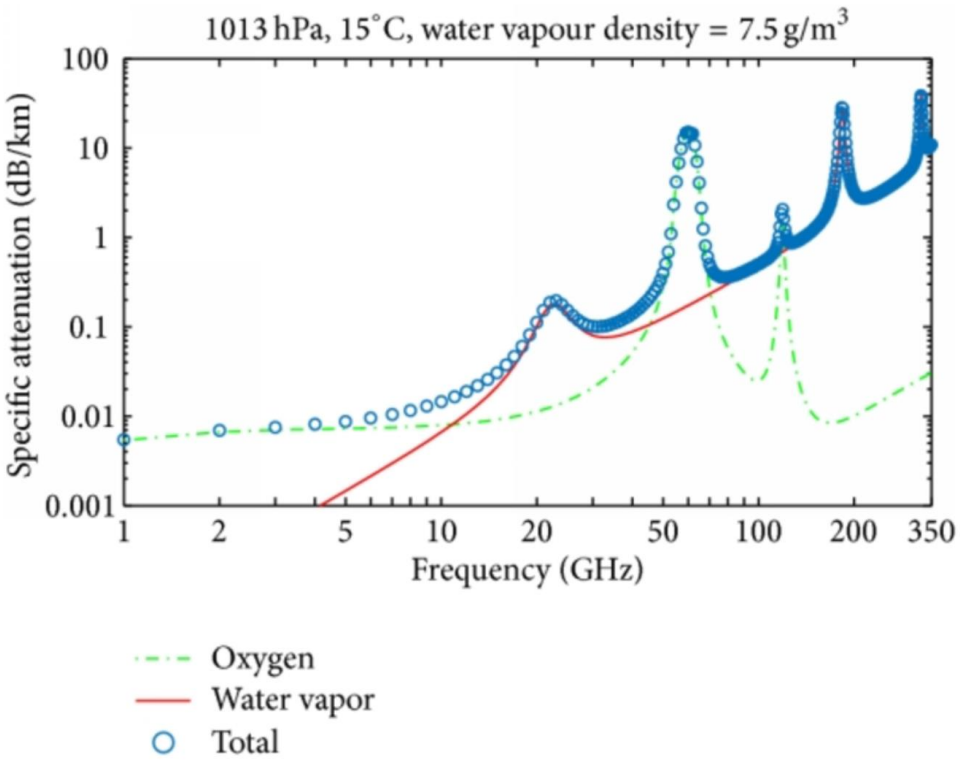

Figure 6. Water and Oxygen Specific Attenuation vs. Frequency [28]

2.2 Radiative Transfer Models

A radiative transfer model is any program that predicts the propagation of electromagnetic radiation in the atmosphere or free space. The Air Force Institute of Technology Center for Directed Energy (AFIT CDE) has developed extensive research and products to calculate the propagation of lasers in the atmosphere to support the ongoing DoD high energy laser research and development. To capture effects such as thermal blooming, optical turbulence, and extinction, programs like LEEDR build an atmosphere from climatology or numerical weather data. This allows for highly accurate determination of parameters that also will affect energy propagated in the RF frequencies.

The atmosphere that LEEDR creates can be ingested into HELEEOS which applies a laser propagation code through that atmosphere to determine irradiance and other laser measures of merit.

This research builds off previous efforts in modeling radar pattern millimeter wave radiation, namely Lt. Richard Cook's Thesis: Capturing Atmospheric Effects On 3-D Millimeter Wave Radar Propagation Patterns. In Lt. Cook's research, several other radiative transfer models were evaluated for use, including APM/AREPS, and IMOM. These models are unable to construct 3-D atmospheric models from real weather data. This capability is critical in studying the impacts of the atmosphere on X-Band power beaming and developing long term attenuation statistics. As a result, these models will not be used.

LEEDR

The AFIT CDE developed LEEDR to build realistic profiles of atmospheric effects which incorporate climatology or numerical weather prediction. The program runs in the MATLAB environment and allows the user to define a wavelength, atmosphere, and scenario geometry (slant angle and altitude). While initially created for high energy laser propagation for the Air Force's Airborne Laser System (ABL), it can provide profiles for temperature, pressure, water vapor content, optical turbulence, and atmospheric particulates and hydrometeors and relate them for EM propagation from the UV to RF. The user can either choose a standard atmosphere, aerosol profile, and weather conditions; or, LEEDR can import data

from a numerical weather prediction (NWP) model using the National Oceanic and Atmospheric Administration's (NOAA) National Operational Model Archive and Distribution System (NOMADS) or climatology database (ExPERT) to provide actual weather conditions at a specific event time.

The atmosphere built by LEEDR is a three-dimensional model and accounts for the change in propagation due to vertical and horizontal (if using NWP) gradients in the atmosphere.

Once LEEDR has built the atmosphere, the path transmittance, path extinction (1/km), surface visibility (km), and slant path visibility (km) for the specific wavelength are calculated by using a line-by-line radiative transfer model. The ability to use a correlated-k method will also increase computation speed, if high spectral resolution is not necessary. Once LEEDR has calculated the atmosphere, it is able to generate a transmittance plot for the path of interest, as shown in Figure 7. This allows one to determine which portions of the spectrum are most opaque and which are transparent for the chosen atmospheric path and conditions [20 and 25].

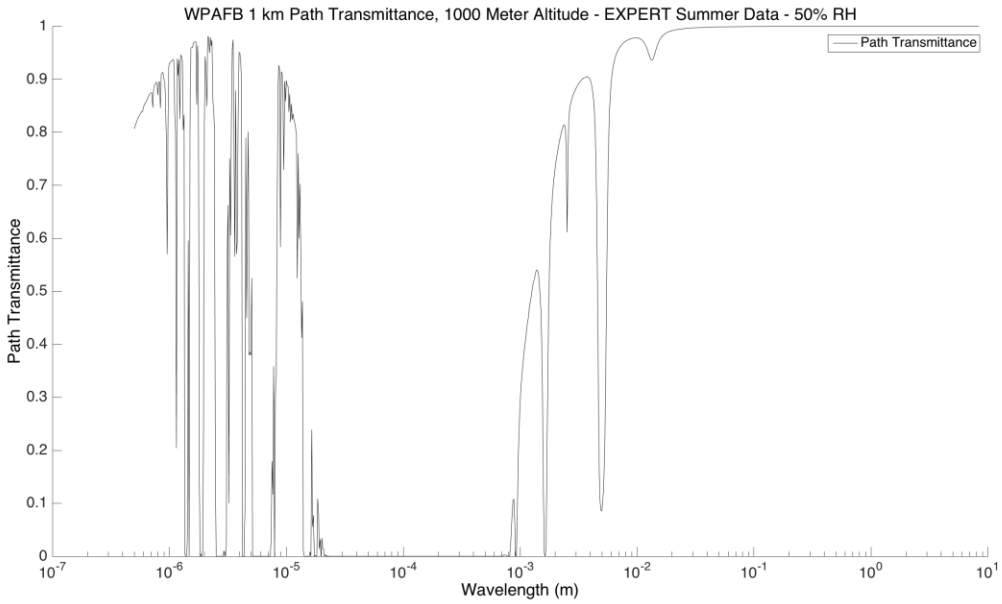

Figure 7. Example of path transmittance calculated by LEEDR for WPAFB at 1200-1500 Local Time During Summer for a 1 km path at 1000 meters altitude [20]

A thorough knowledge of the LEEDR generated atmosphere is necessary in order to understand the assumptions and methods that LEEDR applies to generate the wavelength dependent absorption and scattering of the atmosphere. For molecular absorption, LEEDR considers the constituents and concentrations listed in Table 2. The absorption parameters are calculated using the HITRAN database and using a Lorentz line shape for pressure broadening at wavelengths for less than 1 millimeter. For wavelengths over 1 millimeter, the van Vleck-Weisskopf line shape is used [24].

Table 2. Molecular Absorbers Considered in LEEDR [20]

Absorber	Concentration
H_2O	Variable
CO_2	3.80×10^{-4}
O_3	Variable
N_2O	3.20×10^{-7}
CO	1.50×10^{-7}
CH_4	1.794×10^{-6}
O_2	.209
NO	2.99×10^{-10}
SO_2	2.93×10^{-10}
NO_2	2.99×10^{-11}
NH_3	5.03×10^{-11}
HNO_3	5.30×10^{-11}

For scattering, a number density must be assumed based off particle and droplet sizes. LEEDR uses a log-normal distribution to derive a normalized radius specific particle number density per unit volume as demonstrated in Equation 12. [24]

$$\frac{dN(r)}{d(\log(r))} = \frac{N}{\sqrt{2\pi}\,\log(\sigma)} \exp\left(-(\log(r) - \frac{\log(r_m))^2}{2(\log(\sigma))}\right) \qquad (12)$$

Taking this range of radii, LEEDR integrates over each radius (discretely) to determine a wavelength dependent extinction, scattering, and absorption coefficients for each particle. Using the Wiscombe Improved Mie Scattering algorithm [27], a total attenuation is calculated depending upon particles and atmospheric composition.

$$\sigma_{e,s,a}(\lambda) = \int_{r1}^{r2} Q_{e,s,a}(m,\lambda,r)\pi r^2 \frac{dN(r)}{r \ln 10 d(\log r)} dr \approx \sum_{i=r_{min}}^{r_{max}} Q_{e,s,a}(m,\lambda,r)\pi r^2 \frac{dN_i}{r_i \ln 10 d(\log r_i)} \Delta r_i \qquad (13)$$

These line-by-line and Mie Scattering calculations allow a first principles treatment of radiative transfer in a realistic LEEDR generated atmosphere. For more in-depth analysis and specific equations and assumptions that are included in the LEEDR transmittance calculations, the reader is directed to [24] and the LEEDR Equations and Principles Handbook published by the CDE [4]. Figure 8 gives examples of the end user's GUI for running a LEEDR simulation.

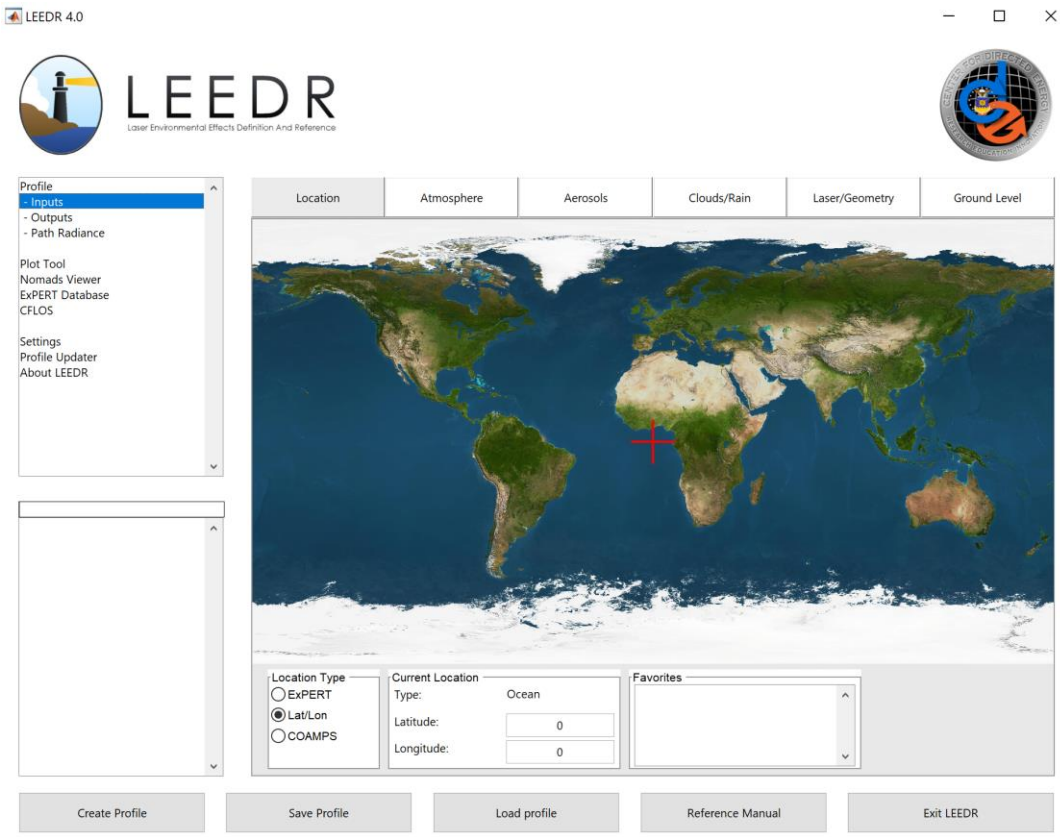

(a) Location Selection for ExPERT or NOMADS Data

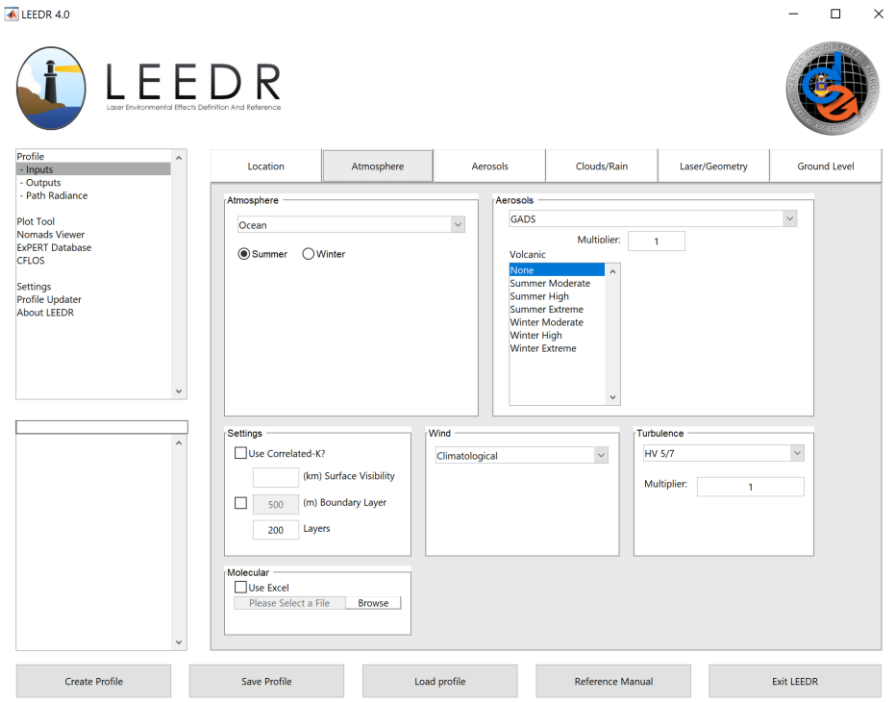

(b) Atmospheric Data Selection

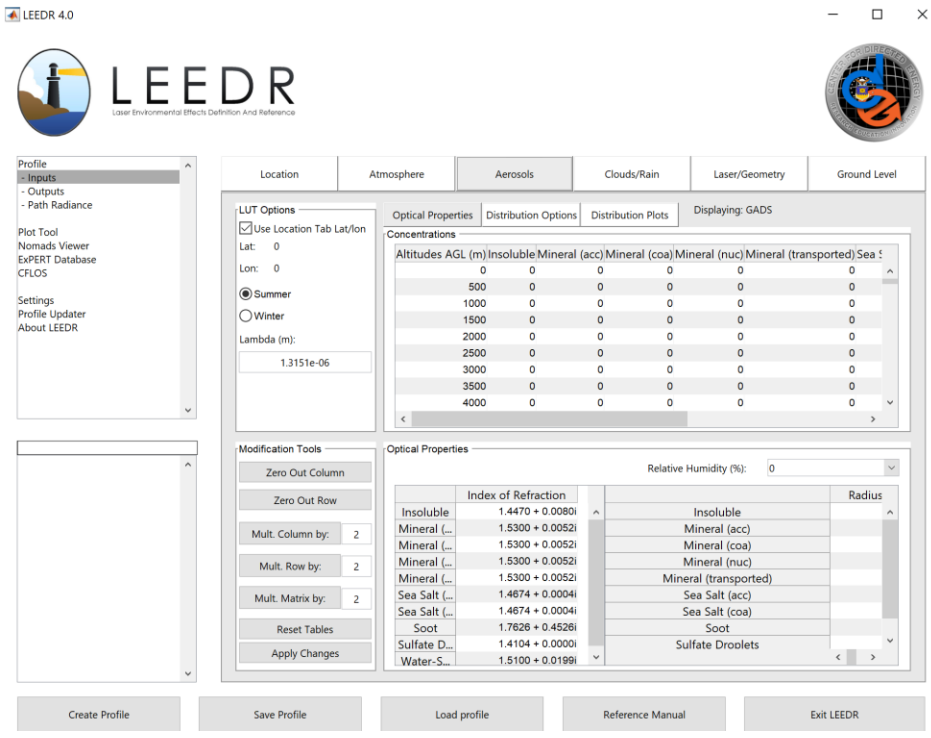

(c) Aerosol Data Selection

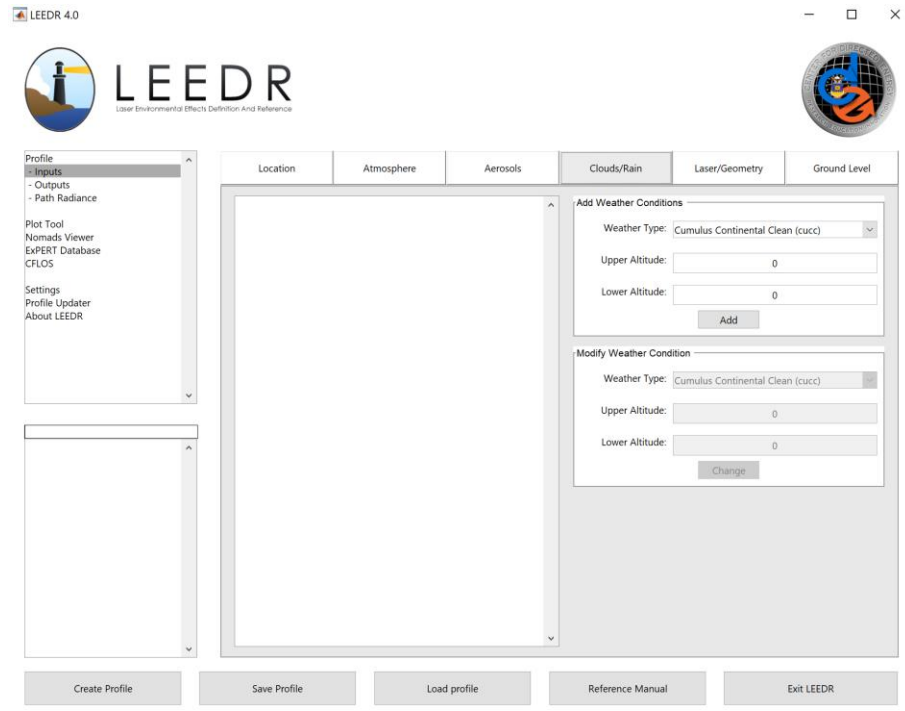

(d) Cloud and Rain Manual Selection

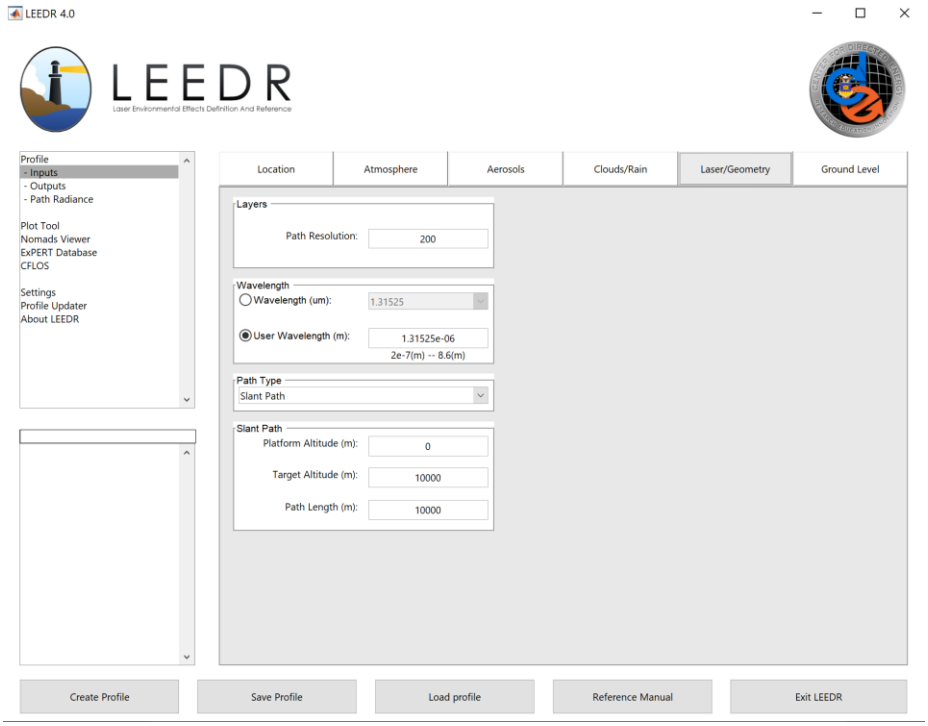

(e) Laser Geometry Information

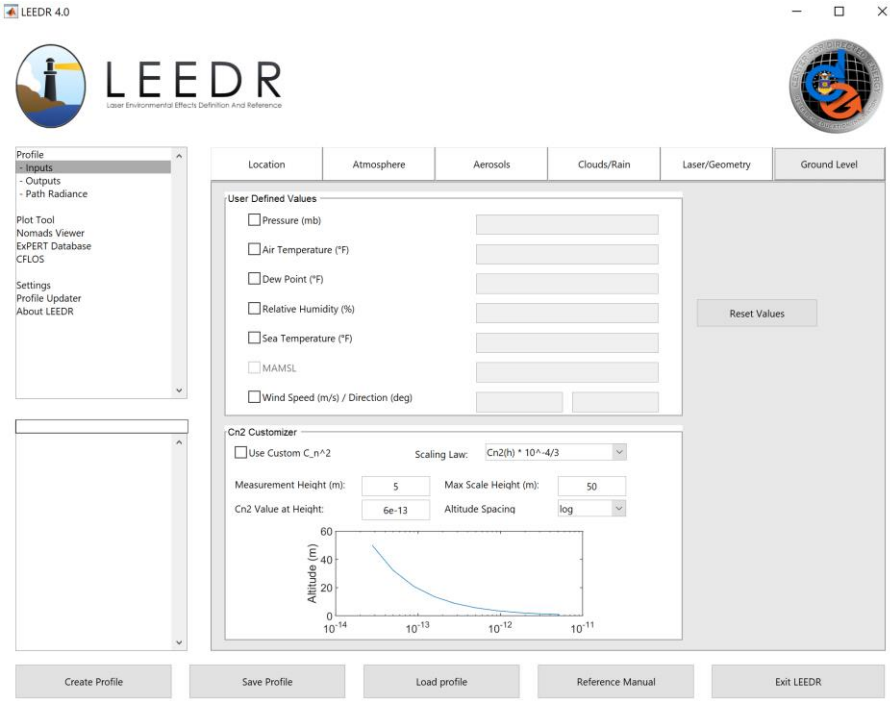

(f) Ground Level Information

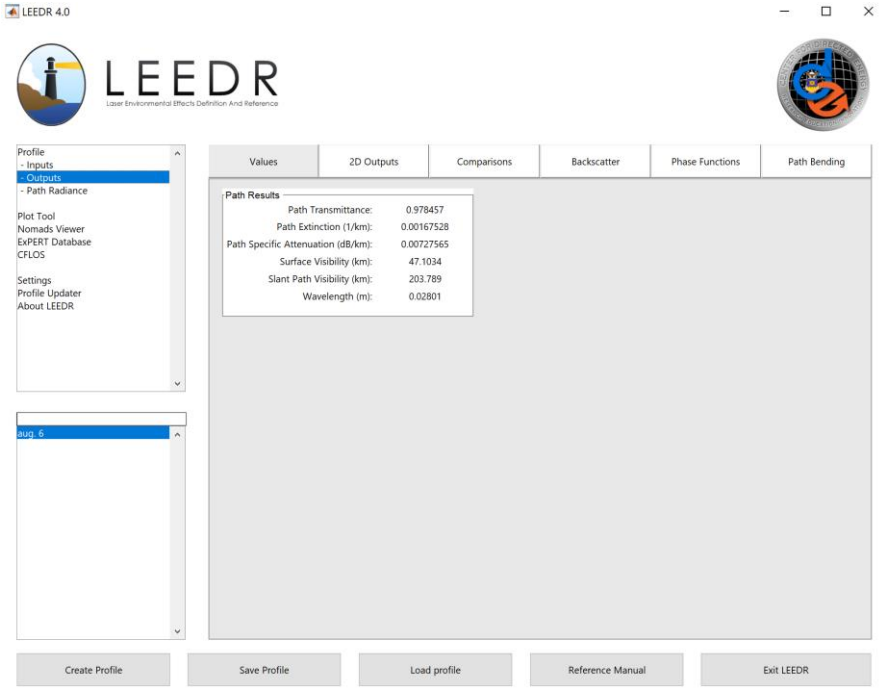

(g) Output Values

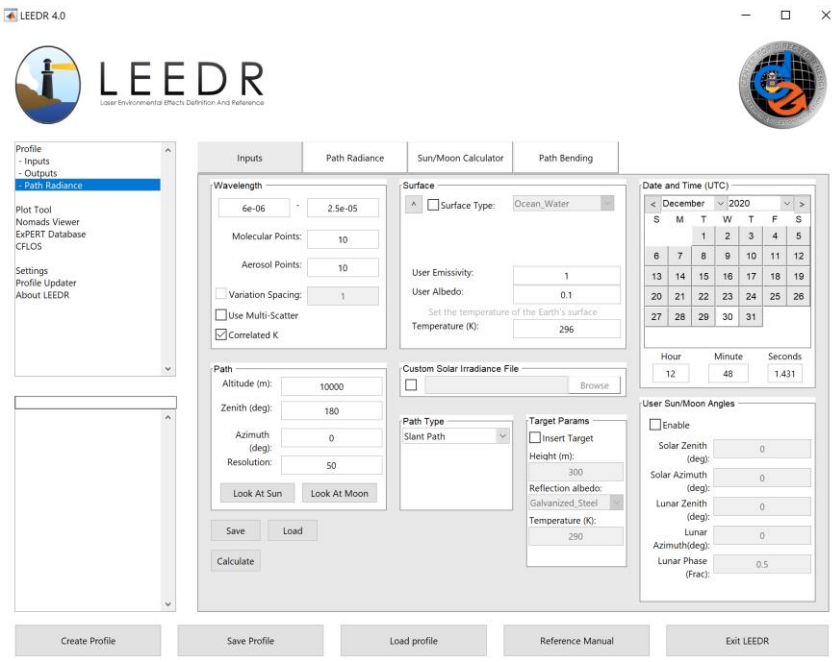

(h) Path Radiance Information

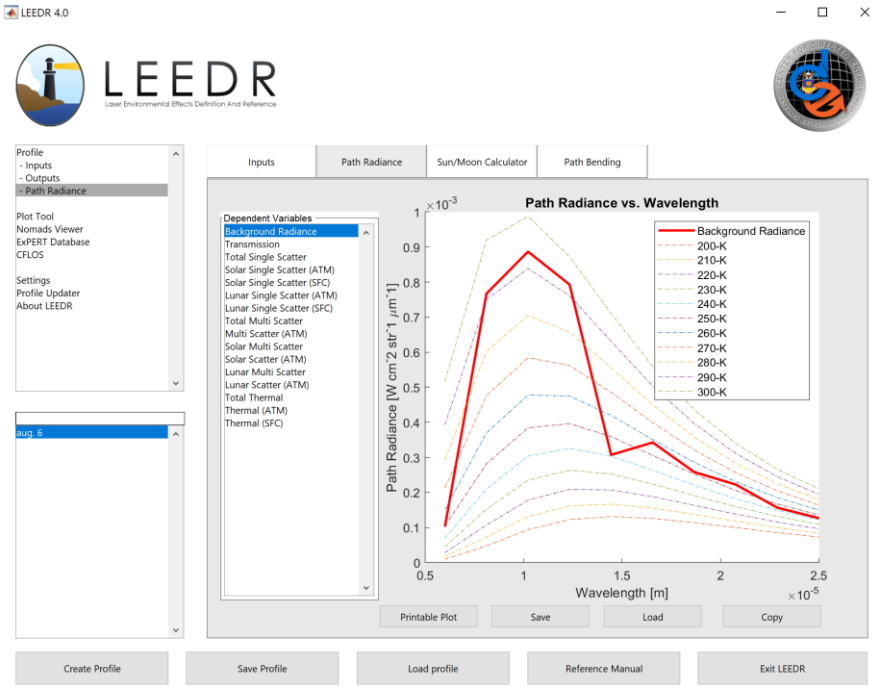

(i) Path Radiance Plots

Figure 8. LEEDR GUI Displays

HELEEOS

HELEEOS builds on the functionality of LEEDR by creating a laser weapon target scenario and determines probability of kill (Pk) along with other laser metrics for a given scenario. HELEEOS uses a wavelength dependent atmosphere built by LEEDR. Additionally, HELEEOS enables the user to specify a laser power, shape, and target type to determine laser operational parameters such as peak irradiance, power in the bucket, spot size, and other interesting measures of merit for laser performance. These fast-calculating values allow for on-the-fly operational assessments for effectiveness of laser propagation. HELEEOS has been well validated and useful in the UV to RF wavelengths. [25].

While traditional extinction makes it difficult to separate the absorption and scattering, HELEEOS treats the two phenomena separate and combines absorption and scattering to provide a total path extinction. Also, HELEEOS provides the scattering information which can, with further research, provide utility in determining off axis radar propagation that could either weaken the beam or allow a radar path more likely to be detected off the area of focus.

2.3 Atmospheric Effects in the X-Band

Weather Effects

The standard dry atmosphere is approximately 78% N2, 21% O2, and 1% other, such as Ar, CO2, and other trace gases [28]. Not included in the dry atmosphere is water vapor (between .001% - 4%), which can greatly affect atmospheric attenuation due to H2O absorption lines. The strong dipole moment present in H2O creates strong

absorption features at 22, 183, and 323 GHz. While these absorption bands are outside the X-Band, they do cause an upward slope of specific attenuation, which begins to occur in the X-Band, as shown in Figure 6.

Suspended Water Droplet Effects

As water droplets grow to become clouds and fog, their scattering properties change (see Figure 3). Therefore, it is important to consider scattering due to fog and clouds, which are defined as droplets with radii less than 100 μm and typically on the order of 10 μm. This places cloud droplets mostly in the Rayleigh scattering regime. Densities of water in clouds are from 1 to 2.5 g/m^3; however, some instances of 4.0 g/m^3 have been reported. For clouds of ice, density is typically less than 0.5 g/m^3 and often can be found at less than 0.1 g/m^3.

Gunn and East [14] created a method to determine the attenuation for a specific wavelength due to cloud droplets in Equation 14 where $\vec{k}$ is defined in Section 2.1 and λ is wavelength in meters.

$$\alpha_{clouds} = 0.4343\frac{6\pi}{\lambda}\frac{\rho_{droplets}}{\rho_{atmosphere}}\mathrm{Im}\left(\vec{k}\right) \tag{14}$$

Due to the sparsity of crystals and small size of ice particles in ice clouds, attenuation may be neglected for consideration of MMW propagation [20].

Precipitation Effects

Rain

Rain droplets are on the same size as X-Band wavelengths which implies approaching Mie Scattering. To account for attenuation due to a specific rain rate, Crane and Blood developed the following Equation to determine attenuation, A, in dB.

$$A = \frac{\alpha {R_p}^{\beta}}{\cos\theta}\left[\frac{e^{u\beta d}-1}{u\beta} - \frac{b^{\beta}e^{c\beta d}}{c\beta} + \frac{b^{\beta}e^{c\beta D}}{c\beta}\right] \quad (15)$$

Where

A = Total Path Attenuation due to Rain (dB)

α, β= Parameters Relating Attenuation to Frequency

R_p= Rain Rate in mm/hr

θ = Elevation Angle of Path ($\geq\ 10^o$)

D= Horizontal Path Distance Through Rain Volume

$$u = \frac{\ln(be^{cd})}{d}$$

b=$2.3R_p^{-0.17}$

c=0.026-0.03ln(R_p)

d=3.8-0.6ln(R_p)

α and β values can be determined from the graph in Figure 14

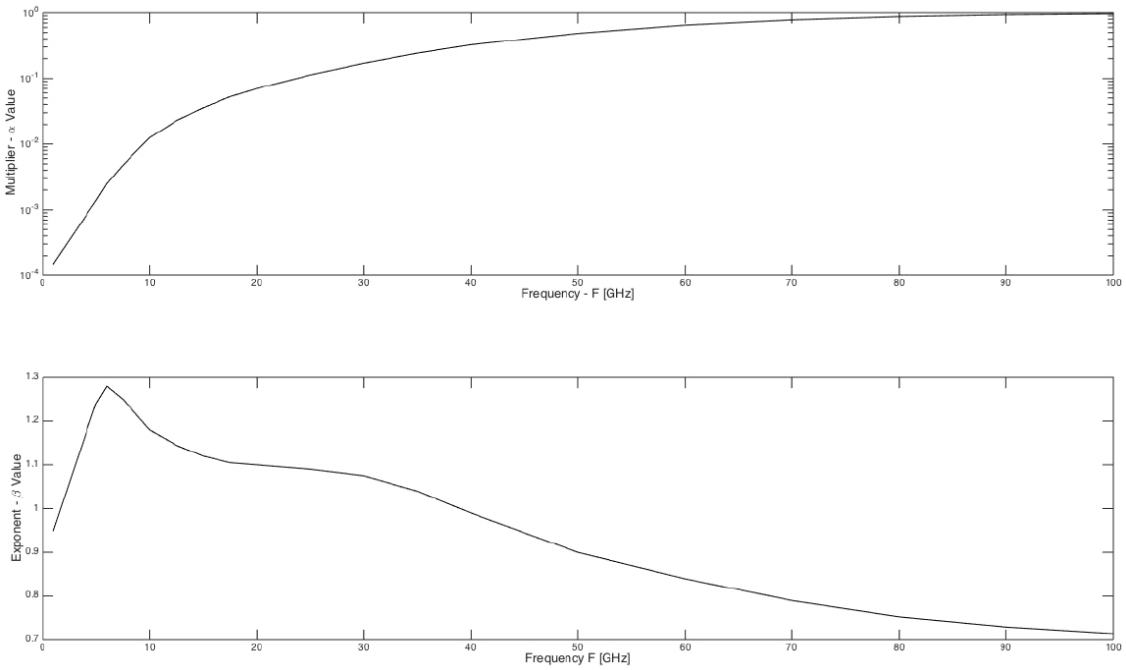

Figure 9. **α and β** Values from Equation 15

If D < d:

$$A = \frac{\alpha R_p^{\beta}}{\cos\theta}\left[\frac{e^{u\beta D} - 1}{u\beta}\right] \tag{16}$$

If D = 0 and $\theta = 90^{o}$

$$A = (\delta H)\left[\alpha R_p^{\beta}\right] \tag{17}$$

Where δH is the path height through the rain area. These Equations provide excellent fitting with measurements in the 1 GHz - 100 GHz range and allow for calculation of attenuation due to rain [22]. The effect of various rain rates are demonstrated in Figure 10(a) and 10(b). Note that as rain rate increases, a nonlinear response to path attenuation arises and the shape of the attenuation versus wavelength curve changes slightly. These effects are vital to capture when propagating X-Band radiation.

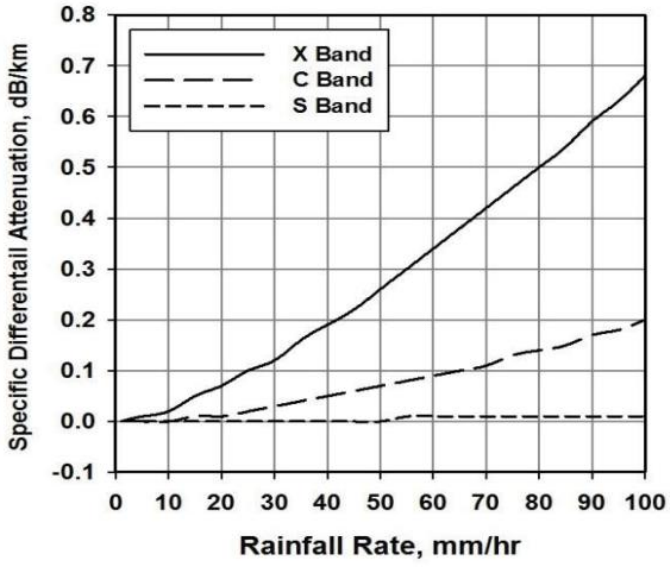

Figure 10a. Specific differential attenuation for X, C, and S bands vs. rainfall rate [6]

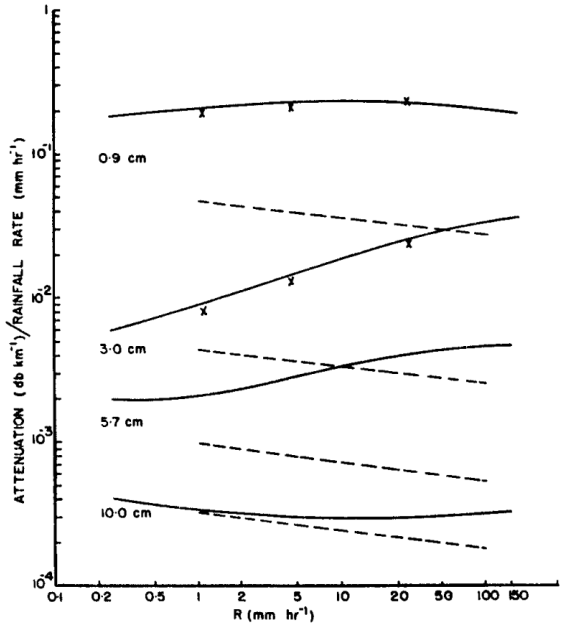

Figure 11b. Attenuation/rainfall rate versus rainfall rate for several wavelengths. The dashed lines show the Rayleigh approximation [14].

Snow

Many assumptions must be made when determining absorption from snow. This is because snow can assume a wide variety of shapes, sizes, types (i.e. wet or dry), and orientations. A proposed method from Nicholas Currie of determining attenuation due to snow is found in Equation 18 [17].

$$\alpha = \frac{0.00349R^{1.6}}{\lambda^4} + \frac{0.00224R}{\lambda} \qquad (18)$$

where R is the snowfall rate in millimeters of water per hour.

From Equation 18, it's clear that the snowfall rate would have to be unnaturally high to be of consequence for X-Band attenuation.

Ice Precipitation

Due to the small size and low density of ice particles, the effect on X-Band attenuation is negligible.

2.4 Validating Models

To validate X-Band LEEDR simulations, its attenuation calculations due to weather will need validating. This methodology will involve using attenuation values to calculate path radiance. This path radiance value will be used in calculating brightness temperatures for comparison against measured events with known brightness temperatures.

Radiance is the radiant flux emitted, reflected, transmitted or received by a given surface, per unit solid angle per unit projected area. This is a directional quantity, measured in $W \cdot sr^{-1} \cdot m^{-2}$. For an in-depth look at how LEEDR calculates path radiance, see the 2019 LEEDR Equations and Principles (LEAP) reference document [4].

Brightness Temperature is the temperature of a black body in thermal equilibrium with its surroundings and is measured in degrees Kelvin. It can be calculated by the inverse Planck Function:

$$T_B(\lambda, L) = \frac{c_2}{\lambda \ln\left(\frac{c_1}{\lambda^5 L} + 1\right)}$$

Where

$c_1 = 1.191042\ x\ 10^8$ (W/ m^{-2} sr·μm^{-4})

$c_2 = 1.4387752\ x\ 10^4$ ($K\ \mu m$)

L= blackbody radiance (W/ m^{-2} sr·μm)

In atmospheric research in several frequency bands, including X, brightness temperatures can be used for estimating the amount of liquid water in the air between the ground and the measurement location. This is easy to do at microwave frequencies over the ocean because the brightness temperature calculations simplify by the Rayleigh-Jeans Approximation, shown in Equation 19.

$$T_B \approx \varepsilon T \qquad (19)$$

Where ε is emissivity, and T is temperature in degrees Kelvin.

If one knew the ocean surface temperature at the location of measurement, then calculating the brightness temperature at the surface would be trivial. From there, one could subtract that value from the measured brightness temperature at a certain altitude, and that difference would the amount of radiation emitters were along that path. In microwave frequencies, emitters are primarily water particles.

2.5 Array Theory

The Air Force Research Laboratory (AFRL) has a proposed design for an X-Band Space Solar Power (SSP) beaming setup, involving an over five million element array of antennas. Given computational limitations of available hardware for this research, it isn't feasible to simulate the entire proposed system, and instead, a single tile, containing 1024 elements would be simulated.

Using Array theory, the results of the single tile could then be used to analytically determine the performance of the entire system.

2.6 Adaptive Optics

A simplistic explanation of Adaptive Optics (AO) for directed energy is using a deformable mirror to reflect a source of radiation through a lens, and then through a propagation medium to a target. The target acts as a beacon, sending a reflected wave back to the source, which has been distorted by the propagation medium, the atmosphere in most cases. These distortions are most commonly due to atmospheric turbulence. The distorted wave passes through the lens, hits a wave front sensor, which then relays the distortions in the wave to the Adaptive Optics computer. The computer then adjusts the deformable mirror to counter-distort the outgoing wave from the directed energy source so that when the next wave propagates through the atmosphere, the atmospheric distortion corrects the wave to the desired shape. A common AO setup for directed energy can be seen in Figure 11 [7].

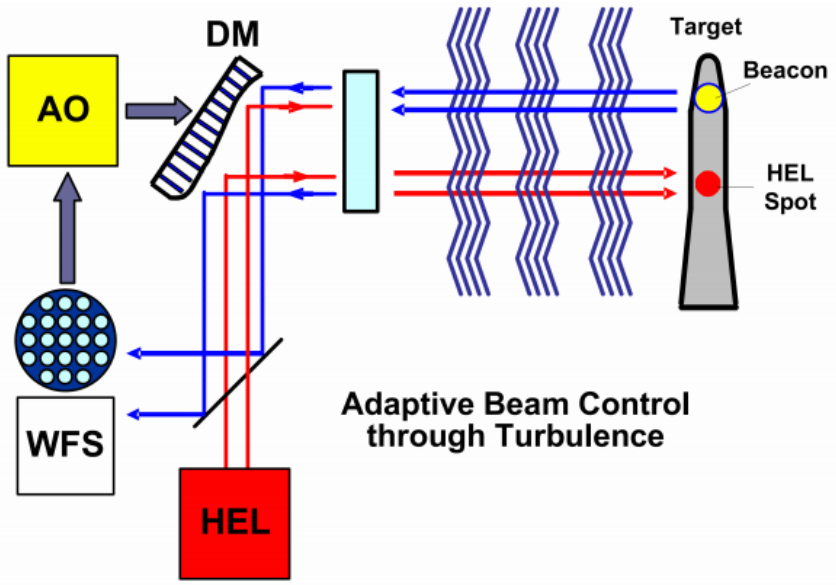

Figure 12. Adaptive Optics Setup For A High Energy Laser. Where AO is Adaptive Optics, WFS is Wave Front Sensor, DM is Deformable Mirror, and HEL is High Energy Laser

For the purposes of X-Band power beaming, AO will not prove helpful. This is determined by looking an estimate for the Fried Coherence Length, r_0.

The Fried coherence length is the transverse distance over which a beam of light will remain coherent, i.e. maintain the same phase difference. It is a function of a specific path through the atmosphere. Coherent light here is generally considered to be light that is in phase within a root-mean-square difference of 1 radian. The Fried parameter for a plane wave is calculated by Equation 20 [7].

$$r_0 = \left[\frac{2.905}{6.88} \left(\frac{2\pi}{\lambda} \right)^2 \int_0^R C_n^2(z) dz \right]^{-3/5} \quad (20)$$

Where

R = Total Path Length

$C_n^2(z)$ = Refractive Index Structure Coefficient

C_n^2 is used to describe atmospheric turbulence, and is governed by pressure and temperature differences, which create an index of refraction difference between two points. The Hufnagel-Valley model can be used to roughly characterize values of C_n^2 as a function of altitude, as shown in Figure 12. A C_n^2 value on the order of $10^{-17}\ m^{-\frac{2}{3}}$ corresponds to weak turbulence while $10^{-13}\ m^{-\frac{2}{3}}$ corresponds to strong turbulence [7].

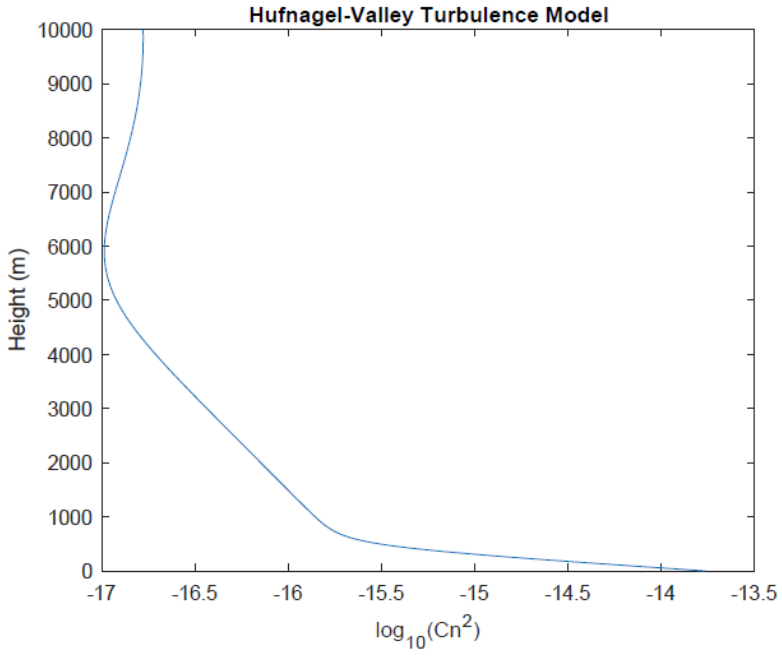

Figure 13. Hufnagel-Valley Model

The altitude dependent $C_n^2(h)$ can be calculated by Equation 21.

$$C_n^2(h) = 5.94 \times 10^{-53}(v/27)^2 h^{10} e^{(-h/1000)} + 2.7 \times 10^{-16} e^{(-h/1500)} + Ae^{(-h/100)} \quad (21)$$

Where:

h = Altitude

v = a high-altitude wind speed

A = C_n^2 near the surface of earth

For X-Band power beaming purposes, one can do a rough calculation of r_0 by putting Equation 21 into 20 and solving. The wavelength will be 3 cm, which correlates to 10 GHz, the path length R will be 500000 m, which correlates to a mid-range low-earth orbit satellite altitude, v will be 125 knots, or 64.3 m/s, which is an average speed of high altitude prevailing winds, and A will be a pulled from Figure 12 to be $10^{-13.75}\ m^{-\frac{2}{3}}$.

$$r_0 = \left(\left(\frac{2.905}{6.88}\right)\left(\frac{2\pi}{0.03}\right)^2 \int_0^{500000} 5.94 \times 10^{-53}\left(\frac{64.3}{27}\right)^2 z^{10} e^{-\frac{z}{1000}} + 2.7 \times 10^{-16} e^{-\frac{z}{1500}} + 10^{-13.75} e^{-\frac{z}{100}} dz\right)^{-\frac{3}{5}} = 27653.53\ m = 27.65353\ km$$

The AFRL proposed system is a 34 by 38 m square antenna array, which has a diameter significantly smaller than 27.65353 km. Because of this significant size difference, it indicates that atmospheric phase changes will be the same at all points across the array, and therefore not need correcting by an AO system. One can also note that using the more correct spherical wave model for calculating the fried parameter

would yield and even larger value for r_0, further emphasizing the lack of need for AO correction.

III. Methodology

Chapter Overview

The purpose of this chapter is to cover in detail the methodology in which LEEDR's attenuation calculations for X-Band radiation are validated against measured data, and how LEEDR is modified to make use of NOAA 1999 climatological data for building simulations.

Validating LEEDR

LEEDR will have its attenuation calculation methods validated via replicating known measured Brightness Temperatures collected during the 1999 Kwajalein Atoll Field Experiment (KWAJEX) [23]. When calculating brightness temperatures, the spectral radiance of the surface of interest must be known, labeled as blackbody radiance in the Inverse Planck Function, in section 2.4. To find the spectral radiance, attenuation must first be calculated. Therefore, if simulated brightness temperatures match well with KWAJEX's measured values, LEEDR's method of calculating attenuation is indirectly validated.

KWAJEX consisted of using a DC-8 aircraft flying at a specific altitude over the Pacific Ocean and using the Advanced Microwave Precipitation Radiometer (AMPR) to measure the brightness temperature of the ocean. The performance characteristics of the AMPR can be seen in Table 3. Although the AMPR operates on 3 different frequencies,

only the 10.7 GHz frequency will be discussed. The AMPR collected data on the dates and times listed in Table 4, generating data files structured as shown in Table 5.

Table 3. AMPR Performance Characteristics [12]

Characteristic	*85.5GHz37.1GHz*	*19.35GHz*	*10.7GHz*
Bandwidth (MHz)	1400900	240	100
Integration Time (ms)	5050	50	50
Horn Type	SSM/ISSM/I	SSM/I	GTRI
Lens Diameter (inches)	5.35.3	5.3	9.7
Beam width (degrees)	1.84.2	8.0	8.0
Footprint (km) [@20 km ER-2 alt. 500kts]	0.641.48	2.78	2.78
Beam Efficiency (%)	N/A98.8	98.7	97.8
Cross Polarization (%)	N/A0.4	1.6	0.2

Table 4. KWAJEX AMPR Flights [12]

Flight Date (UTC)	*Start-stop time UTC*
30 Jul 99	0320-0642
3 Aug 99	0352-0632
6 Aug 99	0320-0512
9 Aug 99	2248-0120
11 Aug 99	2148-0132
14 Aug 99	2332-0044
16 Aug 99	2244-2332
17 Aug 99	1940-2324
19 Aug 99	1940-2316
22 Aug 99	1900-2100
23 Aug 99	0120-0440
24 Aug 99	0324-0556
25 Aug 99	0408-0632
26 Aug 99	0432-0544
28 Aug 99	0332-0508
28 Aug 99	2312-0312
30 Aug 99	2040-2304
1 Sep 99	2340-0140
2 Sep 99	1916-2252
3 Sep 99	0212-0332
4 Sep 99	1908-0042
6 Sep 99	0000-0112
8 Sep 99	0032-0504
8 Sep 99	2054-2244
10 Sep 99	1936-0120
11 Sep 99	1908-2228
12 Sep 99	2252-0044
14 Sep 99	0320-0656

Table 5. AMPR Data Record Structure [12]

Sequence	*Format*	*Size*	*Data type*	*Units*
1	Integer	1	Scan number	none
2	Integer	1	Day of Year	UTC
3	Integer	1	Hour	UTC
4	Integer	1	Minute	UTC
5	Integer	1	Second	UTC
6	Integer	1	QC code (not used)	none
7	real	1	GPS Laltitude	degrees
8	real	1	GPS Longitude	degrees
9	real	1	GPS Altitude	meters
10	real	1	Pitch (+ is nose up)	degrees
11	real	1	Roll (+ is right wing down)	degrees
12	real	1	Yaw (0-360, 0 is N, 90 is E)	degrees
13	real	1	Heading (true)	degrees
14	real	1	Ground Speed	m/s
15	real	1	Air Speed	m/s
16-19	real	4	RMS noise (10, 19, 37, 85 GHz)	Kelvin
20-69	real	50	Pixel TB's at 10.7 GHz	Kelvin
70-119	real	50	Pixel TB's at 19.35 GHz	Kelvin
120-169	real	50	Pixel TB's at 37.1 GHz	Kelvin
170-219	real	50	Pixel TB's at 85.5 GHz	Kelvin
220-269	real	50	Pixel Latitude	degrees
270-319	real	50	Pixel Longitudes	degrees
320-369	integer	50	Mean Sea-level Elevation	meters
370-419	real	50	Fraction Land at 10.7 GHZ Resolution	none

Using NOAA 1999 climatology data [16], a LEEDR simulation atmosphere will be constructed to model, as closely as possible, the environment at AMPR's times of data collection. Table 6 contains the measured climatological parameters available from NOAA.

Table 6. 1999 NOAA Climatological Data Record Structure

File (.1999 – full year)	Variable	Unit
air.2m.gauss	Air temp at 2m	K
Air	Air temp @ pressure	K
Hgt	Geopotential height @ pressure	Gpm
Hgt.sfc	Geopotential height @sfc	Gpm
Land	Land mask	1=land; 0=sea
Mslp	Mean sea level pressure	Pa
omega	Vertical velocity @ pressure	Pa/s
Prate.sfc	Precipitation rate @ sfc	kg/m^2/s
Pres.hcb	High cloud base @ pressure	Pa
Pres.hct	High cloud top pressure	Pa
Pres.lcb	Low cloud base @ pressure	Pa
Pres.lct	Low cloud top pressure	Pa
Pres.mcb	Middle cloud base @ pressure	Pa
Pres.mct	Middle cloud top pressure	Pa
Pres.sfc.gauss	Surface pressure	Pa
Rhum	Relative humidity @ pressure	%
Ugwd.sfc.gauss	U wind @ sfc	m/s
Uwind.10m.gauss	U wind @ 10m	m/s
Uwnd	U wind @ pressure	m/s
vgwd.sfc.guass	V wind @ sfc	m/s
vwind.10m.gauss	V wind @ 10m	m/s
vwnd	V wind @ pressure	m/s

This model will include the location of AMPR data collection, time, altitude, path, frequency, etc. LEEDR will then calculate the path radiance of a 10.7 GHz source radiating in the same setup as the AMPR: a specific altitude, angled at nadir. This path radiance will then be used to calculate brightness temperatures using the inverse planck function shown in section 2.4. These calculated brightness temperatures will then be plotted against KWAJEX measured brightness temperatures. A step-by-step example of these procedures is shown in Appendix B. Results for this method are discussed in detail in Chapter Four.

Modifying LEEDR

Given X-Band radiation's sensitivity to the water content of the air, it is critical to properly model the weather at the time of measurement during the KWAJEX experiment. Fortunately, LEEDR is capable of generating weather cubes from climatology data and predict weather events based on the information, including: rain rates, presence of specific cloud types, and their corresponding altitudes. Unfortunately, 1999 NOAA climatological data is stored in .nc file format. LEEDR was previously unable to utilize this format for the generation of Weather Cubes. As a result, several aspects of the source code were modified for this new capability.

The Weather Cube User Guide outlines the functions of the LEEDR source code [11]. In order to use .nc files for weather cube generation the following LEEDR functions had to be modified: createWeatherCube_300, createWeatherWrapper, getLLLoc, runHydra, wlForTest, and extractedGrb2Profile. Additionally, a new function had to be created to read the .nc data files at times and locations of interest for simulation, called new_nc_reader.

As shown in Table 6, each .nc file has a single parameter's data for all latitudes and longitudes, all times, and all pressure levels if applicable. This arrangement results in large data files, and for the focus of this thesis, much of it is irrelevant. The new_nc_reader function reads a .nc file, determines what weather parameter the data file is associated with, finds the relevant data points collected at the latitude and longitude of interest, the time of interest, and all associated pressure levels.

The 1999 data is low resolution however, only containing data at every half degree latitude and longitude, and only one data point is collected every six hours. To

remedy this, the new_nc_reader function also interpolates data to better approximate parameter values that would be between half degree locations.

The new_nc_reader function is called within the modified extractednetCDF2Profile function. This function calls new_nc_reader many times to read every parameter contained in .nc files needed for weather cube simulations. It then stores the parameter values into a profile and passes the profile onto the function createWeatherCube_300.

The remaining functions' purposes can be viewed on the Weather Cube User Guide [11]. There were few notable changes, to the remaining functions, aside from runHydra. RunHydra is a near-top level function, in which the user inputs the times, locations, and wavelengths of interest for simulation. It then calls the createWeatherWrapper function to make the weather cubes. Previously the function worked with grib2 data files, with their date built into their file name, and used the file names as part of the weather cube iteration process. The function now prompts for user inputs on the date and times to simulate over.

All modified functions, along with much of this research can be found in L:\Research\Terzuoli\Military Students\Noah Friz for future use.

IV. Analysis and Results

Chapter Overview

This chapter discusses weather cube formation issues with available climatology data, and results of LEEDR simulations of KWAJEX data collecting flights.

Weather Cube Issues With Climatology Data

LEEDR was used to simulate the results of several instances of the KWAJEX data collecting flights, however, as shown in Table 5, KWAJEX data does not include climatological data at the time of collection. Additionally, the NOAA climatological data used for LEEDR simulations only include rain rates. This is unfortunate, because LEEDR generated weather cubes proved unhelpful for the prediction of cloud or rain events during the times of interest. NOAA 1999 climatology data is too coarse to provide an accurate model. Six-hour increments between each data point, and half degrees of latitude and longitude between each measured location are not high enough resolution for the creation of useful weather cubes.

Several attempts were made to develop weather cubes for different KWAJEX flight times using this climatology data, however each cube results with a prediction of no clouds, and no rain. This occurs even in cases for which measured brightness temperatures are uncharacteristically high for clear weather. For example, on August 11, a maximum brightness temperature of 282.96 K was recorded by AMPR. On a typical clear day, brightness temperature is normally between 110-140 K. Using the NOAA climatology data available around AMPR's time of measurement, LEEDR constructed a weather cube. Weather cubes are comprised of several meshes, which are discussed in

detail in The Weather Cube User Guide [11]. The wx mesh, or weather event mesh is visually represented in Figure 13. This mesh indicates the location of weather events such as clouds or rain. In Figure 13, the turquoise color indicates a lack of weather events.

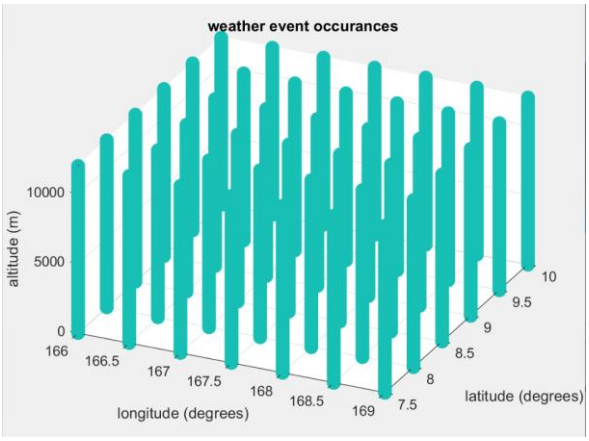

Figure 14. Quantity of Cloud Or Rain Events

Because LEEDR weather cubes are unable to develop useful predictions from such coarse data, simulation weather inputs were developed by a combination of user intuition, and well known cloud behaviors for some tests, and inferences derived from Meterological Aerodrome Reports (METAR) from the airport nearest the KWAJEX site of data collection: Amata Kabua International Airport.

Intuition LEEDR Simulation Results

KWAJEX data collection times were cross referenced with NOAA climatology data point time stamps, to provide six instances of overlap, meaning the AMPR was collecting data at the same time NOAA sensors were collecting climatological data. LEEDR simulations were then ran at these times of overlap to best capture the state of AMPR's experienced weather with the available climatology data.

On August 3, 9, 11, 14, 25, and 29, two LEEDR simulations were created for each date: one without clouds or rain, and one with clouds and rain. The results can be seen in Figure 15. A step-by-step set of these procedures can be viewed in Appendix B

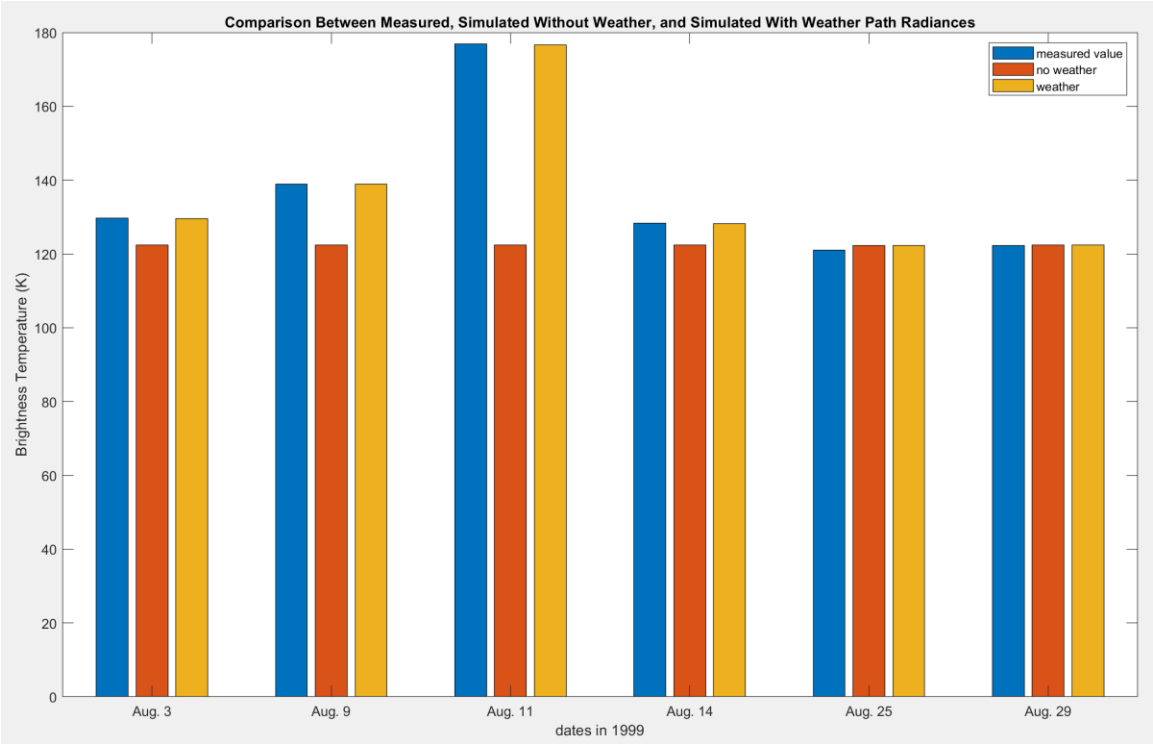

Figure 15. Measured, Simulated Without Weather, And Simulated With Intuited Weather Path Radiances

Based on the results, one can observe excellent agreement between the measured and simulations with clouds and rain to within a hundredth of a degree kelvin at best to 1.5 K at worst. Additionally, one can note reasonable agreement between no-weather simulations and measured results on August 25 and 29.

These results cannot confirm LEEDR's accuracy for modeling X-Band propagation through different atmospheric scenarios, but only further highlight the need for better climatology data to remove the weather condition guesswork. The August 25

and 29 results, do however suggest LEEDR's utility for modeling clear weather scenarios.

METAR Inferred LEEDR Simulation Results

To supplement the weather event predictions normally made by LEEDR weather cubes, METAR data was pulled from the Amata Kabua International Airport collected within 1 hour of KWAJEX's time of data collection [19]. It should be noted that the airport is roughly 224 miles away from the coordinates in which KWAJEX data was collected, and therefore not an exact representation of the weather experienced. Inferences were then made from the METAR data to develop weather scenarios for the same August dates tested in Figure 15.

From these reports, the only information used in developing the LEEDR simulation profile was: observed clouds and rain rates, overall weather (overcast, clear skies, etc), cloud ceilings, and heights at which cloud coverings were broken, scattered, or clear. NOAA climatology data was still used to for other parameters of LEEDR simulations. The nature of these reports is largely ambiguous, only giving a vague idea for the weather, still leaving a large amount of guess work. The results are shown in comparison to previous results, in Figure 16. It should be noted that the August 25 and 29 tests had no weather inputs, and therefore match exactly to the No Weather and Intuited Weather tests. The raw data from which Figures 15 and 16 are developed can be viewed in Appendix C.

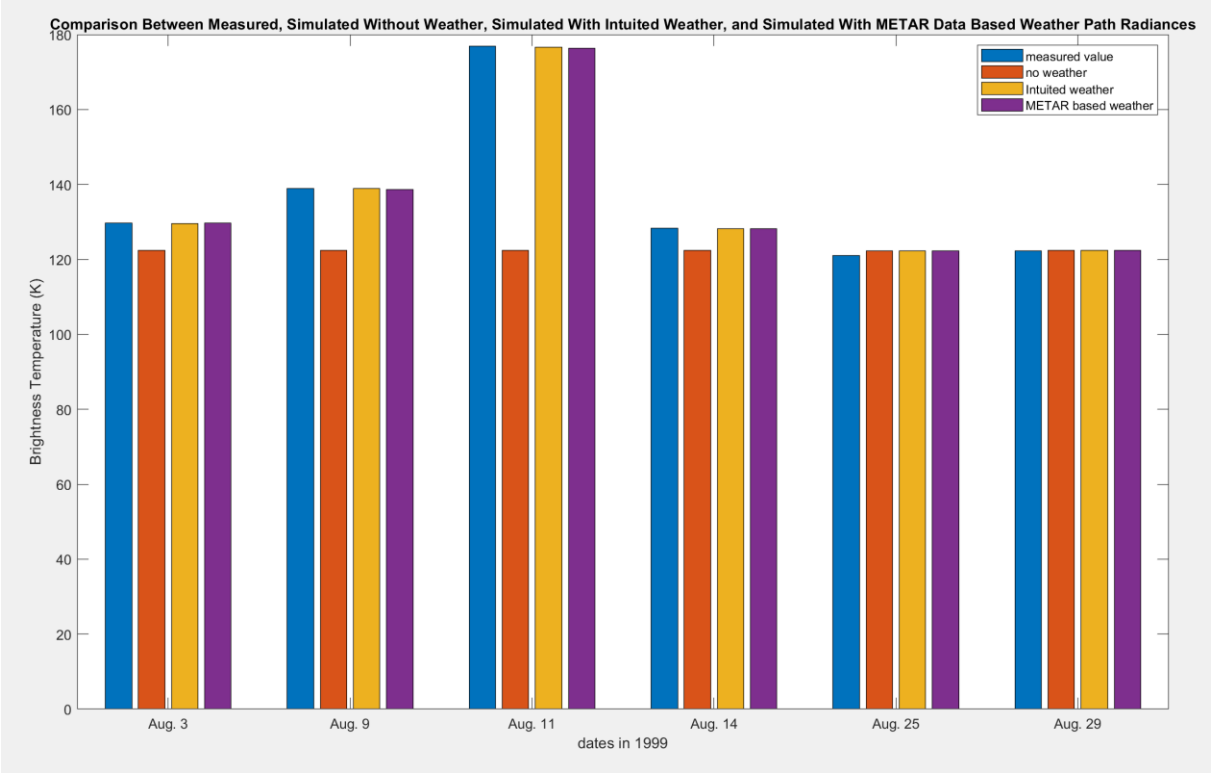

Figure 16. Measured, Simulated Without Weather, Simulated With Intuited Weather, and Simulated With METAR Inferred Weather Path Radiances

High Brightness Temperature Simulations

On August 11, 1999 at 2158, AMPR recorded its largest brightness temperature measurement, 282.96 K. This value correlates to a path radiance of 3.807 e-12 W/(m^2*sr*um). The closest corresponding climatological data was collected two hours and two minutes later. A LEEDR simulation was made to replicate this maximum brightness temperature using procedures covered in appendix B. This resulted in a brightness temperature of 133.05 K. In an attempt to increase brightness temperatures further, nine simulations were ran with weather scenarios each more intense, and unlikely to occur than the last. The results of these simulations can be seen in Figure 17.

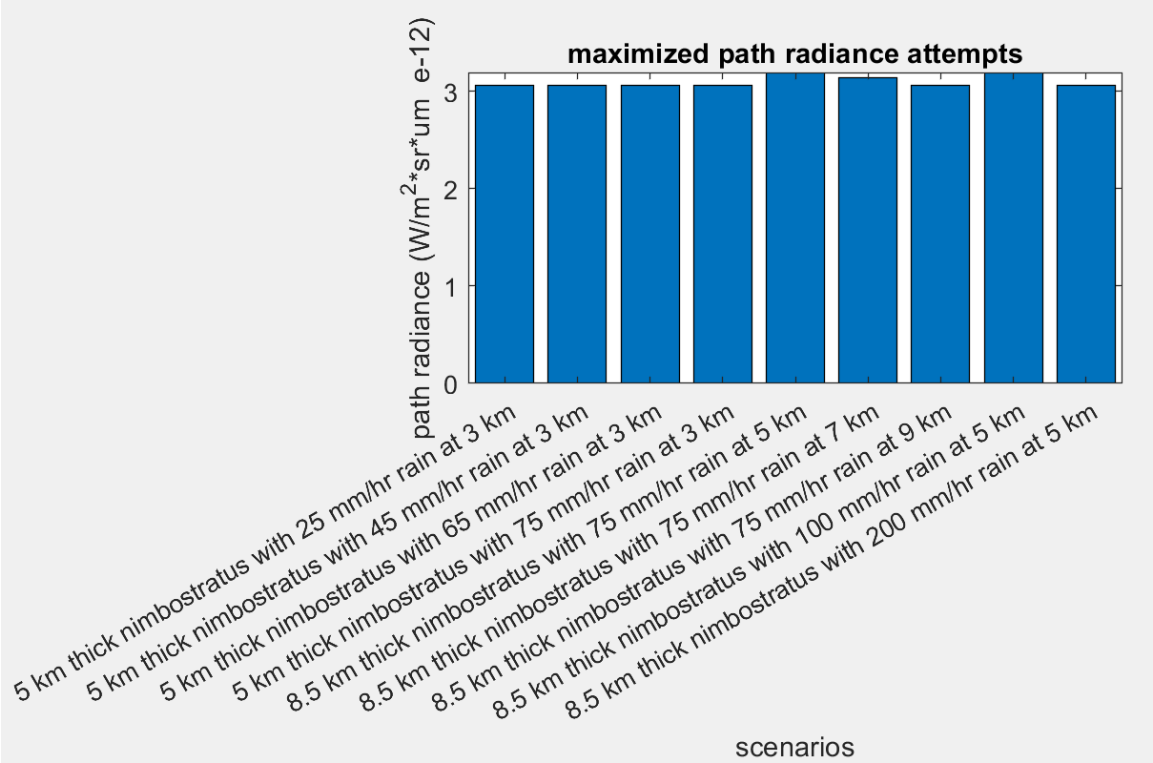

Figure 17. August 11, 1999 Maximum Brightness Temperature Simulation Attempts

From these, the highest simulated value LEEDR could produce for any weather scenario was 3.1919 e-12 W/(m^2*sr*um), which correlates to a brightness temperature of 237.25 K. This leaves a difference of 45.71 K between the measured and simulated value, and makes apparent that adjusting these settings alone within LEEDR is not sufficient for modeling more complex weather scenarios.

Another set of simulations to match the maximum measured brightness temperature was then ran. This time, an emphasis was placed on maximizing the water content of the clouds, and adjusting microphysical qualities in addition to the parameters covered in Appendix B. The microphysical parameters adjusted within LEEDR can be seen in Figure 18.

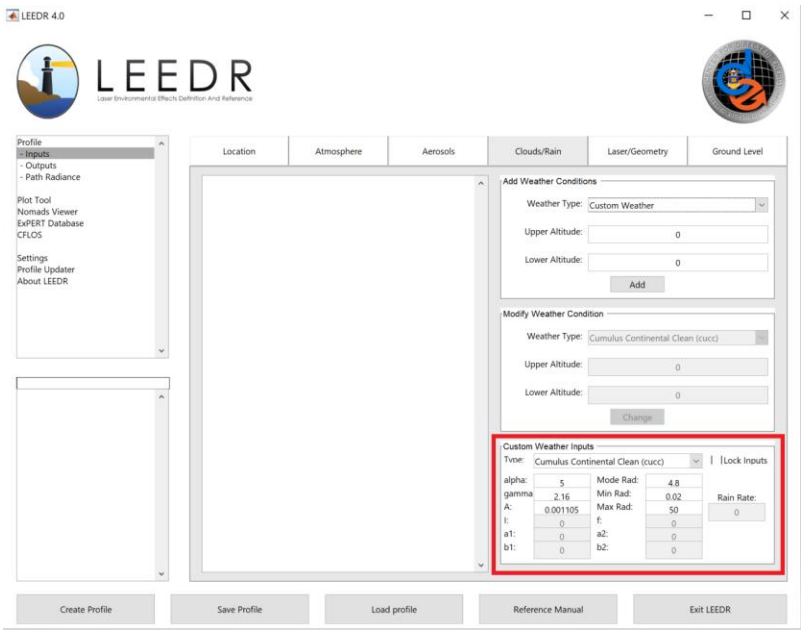

Figure 18. Microphysical Parameters in LEEDR

The non-grayed-out terms correlate to the modified gamma distribution LEEDR uses to model clouds, shown in Equation 22. The cloud modeling methodology is discussed in more detail in [15].

$$\frac{dN}{dr} = Nar^{\alpha} \exp\left[-\frac{\alpha}{\gamma}\left(\frac{r}{r_{mod}}\right)^{\gamma}\right] = Nar^{\alpha} \exp[-Br^{\gamma}] \qquad (22)$$

Where

$$B = \frac{\alpha}{\gamma r_{mod}^{\gamma}}$$

N = the total number density in particles per cm^3

a = the normalization constant ensuring the integral of the size distribution over all radii equals N

α and γ describe the slope of the cloud particle slope

r_{mod} is the mode radius in micrometers

To maximize the water content, the parameter "a" for a maritime cumulus cloud was increased by a factor of roughly 15, its base altitude set to 500 m, and its thickness was set to 5500 m to simulate a towering cumulus cloud. Additionally, the relative humidity of the atmosphere was increased to the 99^{th} percentile, and rain drop radii was set to a range of 50 – 2000 um. Rain was placed at 4000 m, and set to 75 mm/hr. With these settings, a brightness temperature of 267 K was achieved, still low by 16 K.

The influences of the microphysical weather parameters are highly nuanced. For example, rain drops are known to be smaller in radius as altitude increases. LEEDR however, does not capture this relationship within its code. Instead, rain is modeled as a homogenous range of radii at every altitude. A background in meteorology is essential for incorporating these qualities into weather simulations for increased accuracy, if developing simulated atmospheres from data sets which don't include these parameters, such as the 1999 NOAA set. Even when adjusting a number of these microphysical qualities, LEEDR is still unable to reach the desired maximum brightness temperature, instead approaching a value of 270 K.

Power Beaming Applications

Although the inability to match simulated temperatures to the maximum measured temperature seems problematic at first glance, LEEDR's approximate 270 K asymptote due to water saturation actually aligns well with trend lines developed from other studies with radiometers on brightness temperatures for 10 GHz radiation, as shown in Figure 19a and 19b [23] and [21]. With these figures, it becomes apparent that brightness Temperatures above 280 K are outliers from the trend line. Additionally, in all the

thousands of KWAJEX data points, only 21 instances of brightness temperatures above 280 K occur, all of which were on August 11, further illustrating the outlier nature of this maximum value.

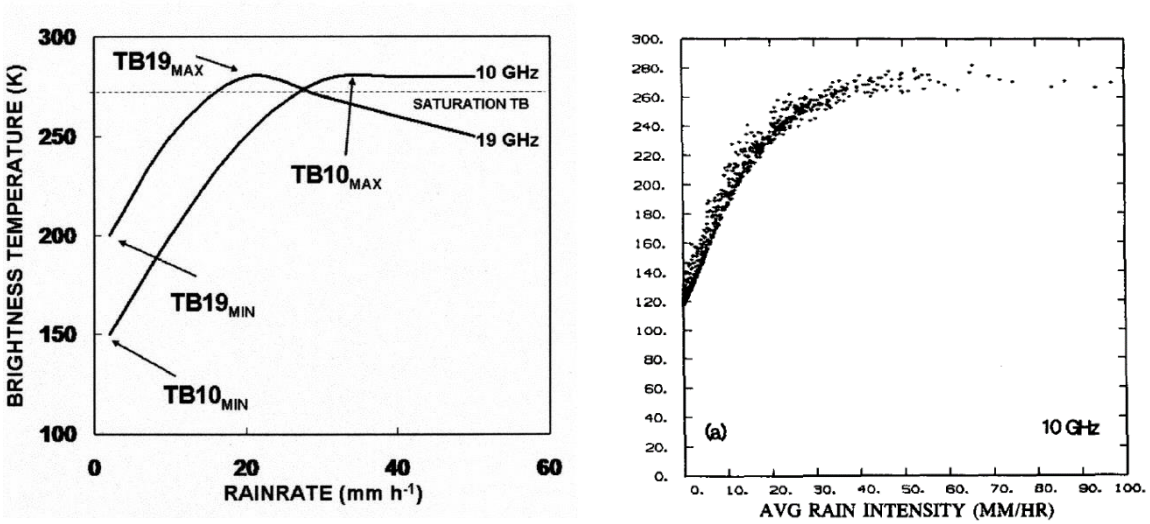

(a) (b)

Figure 19. Rain rate vs. Brightness Temperatures for 10 GHz radiation. (a) is from [23], (b) is from [21]

The curves shown in Figure 19 can be approximately recreated in LEEDR, as shown in Figure 20. This plot was generated by following procedures in Appendix D. Although this recreated plot was not generated from climatology data, each plot point has an associated total extinction value, and transmission value calculated from well known, and validated first principles, discussed in detail in [4]. The associated extinction and transmission values are shown in Figures 21 and 22 respectively.

For a setup such as a 10 GHz power beaming satellite, one could attach a 10 GHz radiometer to its setup and measure the brightness temperature for the transmission path

of interest in real-time. One could then quickly relate the brightness temperature to the associated extinction and transmission values shown in Figure 21 and 22 to determine how well the beam would propagate.

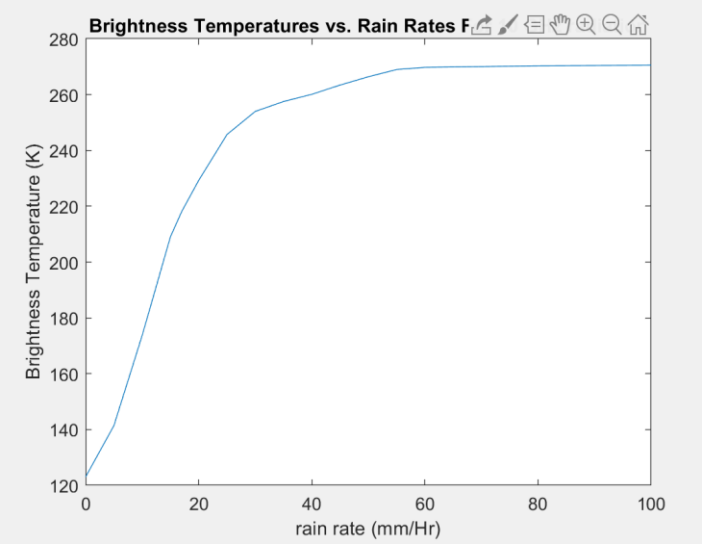

Figure 20. LEEDR Generated Rain rate vs. Brightness Temperatures for 10 GHz Radiation Along a 100 km Nadir Path.

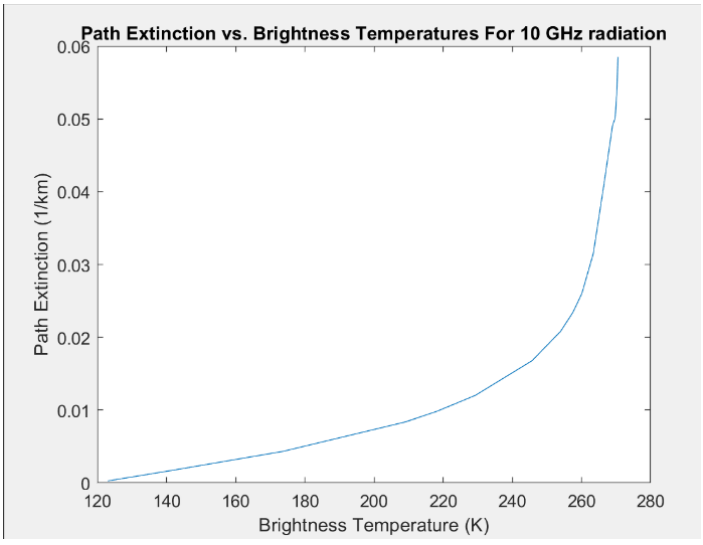

Figure 21. LEEDR Generated Path Extinction vs. Brightness Temperature for 10 GHz Radiation Along a 100 km Nadir Path

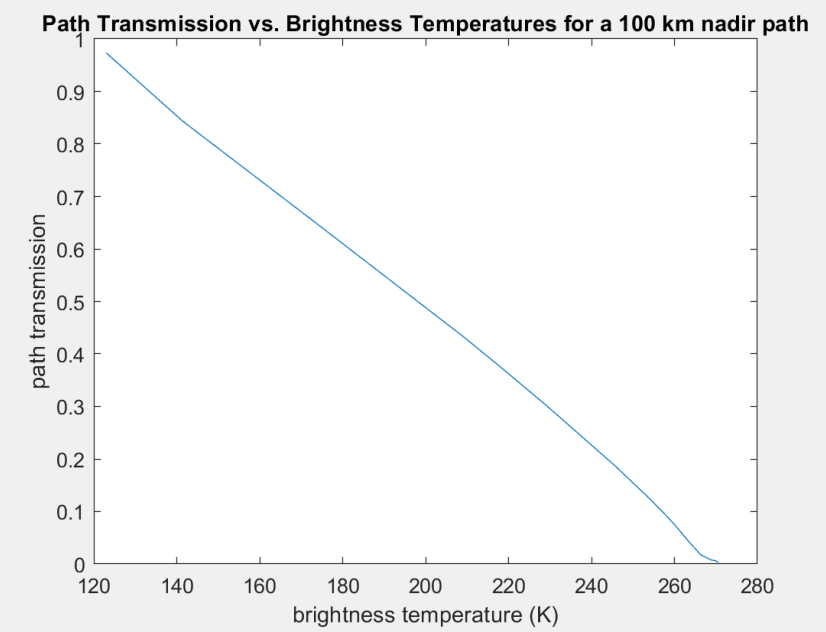

Figure 22. LEEDR Generated Path Transmission vs. Brightness Temperature for 10 GHz Radiation Along a 100 km Nadir Path

This capability could be applied to any frequency within the X-Band with measured brightness temperatures to rain rate curves, which LEEDR could then replicate, and calculate the associated extinction value.

V. Conclusions and Recommendations

Chapter Overview

This chapter discusses the need for higher resolution data to more conclusively validate LEEDR for X-Band radiation propagation and discusses the potential ways to accomplish it. A way to attain approximate attenuation levels in real time for a power beaming satellite is also covered.

Conclusions of Research

This study was unable to conclusively validate LEEDR's ability to accurately model X-Band propagation through Earth's atmosphere via replicating brightness temperatures observed during KWAJEX. The climatology data available during 1999 is too coarse to build a LEEDR atmosphere which accurately captures the state of the environment in which KWAJEX collected data or develop useful weather cubes to infer the presence of cloud or rain events.

Despite an inability validate conclusively, LEEDR does demonstrate promise for modeling X-Band radiation. As shown in Figure 15, a user is able to consistently attain good agreement between measured and simulated brightness temperatures by modifying the simulated atmosphere for lower brightness temperature scenarios, which correlate to less intense weather patterns, such as light rain, partly cloudy, clear weather, etc. With higher resolution data, LEEDR could develop weather cubes, and infer the existence and location of cloud or rain events, which would help tremendously in capturing the atmosphere at a time of interest.

Additionally, this study highlighted the level of nuance, and impact microphysical weather parameters have on microwave brightness temperatures, such as cloud droplet size distributions, rain drop radii, and the number of water particles in the air. In order to properly model the atmosphere during events such as thunderstorms, climatology data used in LEEDR simulation building would have to include these difficult to measure parameters, and more precisely cover cloud and rain events. Without these parameters, simulation building falls to user intuition and guesswork, for which a background in meteorology is needed to do well.

Although imperfect data impedes perfect atmospheric replication within LEEDR, the software utilizes well known and validated first principles when calculating path radiance, and therefore brightness temperatures. Using LEEDR, the rain rate vs. brightness temperature curves developed in two separate studies for 10 GHz radiation shown in Figure 19 was replicated. This replicated curve can be seen in Figure 20. In recreating this curve, LEEDR calculates path transmittance and path extinction values associated with each brightness temperature data point.

By attaching a radiometer to the AFRL proposed SPS, one could easily measure the brightness temperature of the intended propagation path for the power beam, then using the data table generated by LEEDR for the curve shown in Figure 20, one could look up the associated transmittance and extinction values, and thus get a good approximation for how much power the beam can expect to transmit. This capability would give a real time approximation for transmission efficiency and be invaluable for tactical decision making for wirelessly powering global operations.

Significance of Research

Although this study failed to conclusively validate LEEDR's ability to simulate the propagation of X-Band radiation through the atmosphere, it succeeded in showing its potential to do so. Should a future study build on this one, and prove conclusively LEEDR's capabilities, the Air Force would have a powerful tool for modeling the attenuation of X-Band radiation anywhere in the world, for any weather scenario. This capability would be invaluable in analyzing the feasibility, and efficiency of future X-Band power beaming technologies.

Recommendations for Action

It is recommended a more recent study on X-Band atmospheric propagation, occurring on 2015 or later, be found and replicated within LEEDR. This would allow LEEDR to use higher resolution climatology data in developing weather cubes and more accurate atmospheres. Similar efforts could then be carried out as in this research to conclusively prove LEEDR's validity in the X-Band.

If no such study is available, finding higher resolution climatology data for 1999 around Kwajalein-Atoll Island will be critical for conclusive validation via the KWAJEX study. A potential option may be found through the European Centre for Medium-Range Weather Forecasts (ECMWF) and their ERA5 data, which has climatology data points taken on a 0.25x0.25 degree grid all over Earth, taken every hour, as opposed to the 0.5x0.5 degree grid, every six hours data sets which NOAA offers [10]. ERA5 data is available in NetCDF (.nc) format, meaning it could be used by the modified LEEDR code to develop weather cubes. However, as of now the ERA5 data in this format is experimental, and currently incompatible with LEEDR. This may change in the future, but there is another option. ERA5 data is also stored in GRIB file (.grb) form, a format LEEDR doesn't currently take. It may be possible to modify LEEDR to accept .grb files, just as it was changed to accept .nc files.

Recommendations for Future Research

Should LEEDR be validated for the X-Band, and prove able to accurately model X-Band radiation through different weather scenarios, it is recommended HELEEOS be employed to model the AFRL antenna array's beam pattern. From there, one could

simulate this beam's propagation through many different locations and weather scenarios to attain long-term attenuation statistics.

Appendix A

```
function [parameter_data] =
new_nc_reader(filename,parameter,lat,lon,time)
%.nc fole reader
%files and extracts info for the time and place correlated to the
latitude
%range, longitude range, and time range (in hours from jan. 1,
1800)

%lat is the latitude coordinate of interest
%lon is the longitude coordinate of interest

%time is the time of interest
%On september 15 at 2359, time is 1750543 hours

%filename is the 'nameofthefile.nc'

%parameter is the string form of the parameter you want to look
at in the
%.nc fil. for example, in the prate.sfc.gauss.1999.nc it is prate
(or
%precipitation rate)

% To get information about the nc file
%ncinfo(filename)
% to display nc file
%ncdisp(filename)
% to read a vriable 'var' exisiting in nc file
myvar = ncread(filename,parameter);

if lon < 0
   lon = lon + 360;
end

%read the nc file for latitude and longitude arrays. Transpose
for
%calculation later
all_lats=ncread(filename,'lat')';
all_lons=ncread(filename,'lon')';

[latm, lonm] = meshgrid(all_lats, all_lons); % This creates an
NxM grid representative of the pairings between the lat and lon
vectors.
[arclen, ~] = distance(lat, lon, latm, lonm); % first 2 inputs
are single values, not vectors or matrices.

% Find the closest row/col indices to the selected lat/lon
[row, col] = find(min(min(arclen)) == arclen);
```

```
% Choose an area based on the current lat/lon. This ensures we
% properly encapsulate the selected lat/lon.
rows = unique(clip(row, 1, 'min'):clip(row, size(lonm, 1),
'max'));
cols = unique(clip(col, 1, 'min'):clip(col, size(lonm, 2),
'max'));

%choose a time closest to desired time
all_time=ncread(filename,'time');
[minValue, closestIndex] = min(abs(time - all_time.'));
time = all_time(closestIndex);


%% this section trims the 3-d array to only have stuff we're
interested in for precipitation rates
%precipitation rate is a 3-D array of lon, lat, time

if strcmp(parameter,'prate')
precipitation=double(myvar(rows,cols,closestIndex));
parameter_data=precipitation;

%% this section trims the 4-d array to only have stuff we're
interested in for air temperature
%air temperature is a 4-D array of lon, lat, level (pressure),
time

elseif strcmp(parameter,'air')
airtemp=double(myvar(rows,cols,:,closestIndex));
parameter_data=airtemp;

%% this section trims the 4-d array to only have stuff we're
interested in for relative humidity
%relative humidity is a 4-D array of lon, lat, level (pressure),
time

elseif strcmp(parameter,'rhum')

rhum=double(myvar(rows,cols,:,closestIndex));
parameter_data=rhum;
level=ncread(filename,'level');


%% this section trims the 3-d array to only have stuff we're
interested in for precipitation rates
%precipitation rate is a 3-D array of lon, lat, time

elseif strcmp(parameter,'pres')

pressure=double(myvar(rows,cols,closestIndex));
parameter_data=pressure;
```

```
%% this section trims the 4-d array to only have stuff we're
interested in for height
%height is a 4-D array of lon, lat, level (pressure), time

elseif strcmp(parameter,'hgt')

hgt=double(myvar(rows,cols,:,closestIndex));
parameter_data=hgt;

%% this section trims the 4-d array to only have stuff we're
interested in for u-winds
%uwnd is a 4-D array of lon, lat, level (pressure), time

elseif strcmp(parameter,'uwnd')

uwnd=double(myvar(rows,cols,:,closestIndex));
parameter_data=uwnd;

%% this section trims the 4-d array to only have stuff we're
interested in for ground u-winds
%ugwd is a 3-D array of lon, lat, level, time

elseif strcmp(parameter,'ugwd')

ugwd=double(myvar(rows,cols,closestIndex));
parameter_data=ugwd;

%% this section trims the 4-d array to only have stuff we're
interested in for v-winds
%height is a 4-D array of lon, lat, level (pressure), time

elseif strcmp(parameter,'vwnd')

vwnd=double(myvar(rows,cols,:,closestIndex));
parameter_data=vwnd;

%% this section trims the 4-d array to only have stuff we're
interested in for ground v-winds
%vgwd is a 3-D array of lon, lat, level, time

elseif strcmp(parameter,'vgwd')

vgwd=double(myvar(rows,cols,closestIndex));
parameter_data=vgwd;

%% this section trims the 4-d array to only have stuff we're
interested in for vertical velocity
%veritcal velocity is a 4-D array of lon, lat, level (pressure),
time
```

```
elseif strcmp(parameter,'omega')

omega=double(myvar(rows,cols,:,closestIndex));
parameter_data=omega;

else

end
```

Appendix B

Brightness Temperature Calculation Methodology:

This document is a step by step method of an attempt to replicate the measured results of AMPR data file: kwajex_ampr_19990806_ghrc_ver2.txt

This data was collected on august 6, 1999 from 0320 to 0512,
At latitude: 7.99-9.36 degrees
At longitude: 167.17-168.77 degrees
At altitude: 1.1371e4 – 1.0055e3 meters

To do this, the data from the .txt file is first loaded into a custom MATLAB script called data_file_trimmer.m. This script reads the entire data file, removes irrelevant data from the study for ease of navigation, and places the relevant data in an easily read cell array called T_Cell.

The last column of this cell array contains the brightness temperature of the 10.7 GHz measurement suspected to be at nadir. The values contained here are what we're attempting to match calculated values with.

Next we move onto extracting real weather data from NOAA data tables, which will be used to set the parameters for the LEEDR simulation.

Extracting Data From NOAA Tables

This is done using a custom MATLAB function titled test_reader, which reads the .nc files the NOAA data is stored in, and interpolates over the data points to provide weather parameter values that most closely approximate the value at the time and location of interest for the simulation.

This function has 5 inputs:

- .nc file name
    - This is string input which is the full name of the file to be read.
- The data parameter of interest
    - This is a string input which must be the file's name for the parameter of interest
- The latitude of interest
    - This is a single numerical value which is the latitude of interest
- The longitude of interest

    - This is a single numerical value which is the longitude of interest
- The time of interest
    - This is a single numerical value representing the time of interest. However, the time is measured in the number of hours since January 1, 1800. This value can be calculated by this website: https://www.convertunits.com/dates/

NOAA has the following parameters that can be used for use in building the LEEDR simulation:

File (.1999 – full year)	Variable	Unit
air.2m.gauss	Air temp at 2m	K
Air	Air temp @ pressure	K
Hgt	Geopotential height @ pressure	Gpm
Hgt.sfc	Geopotential height @sfc	Gpm
Land	Land mask	1=land; 0=sea
Mslp	Mean sea level pressure	Pa
omega	Vertical velocity @ pressure	Pa/s
Prate.sfc	Precipitation rate @ sfc	kg/m^2/s
Pres.hcb	High cloud base @ pressure	Pa
Pres.hct	High cloud top pressure	Pa
Pres.lcb	Low cloud base @ pressure	Pa
Pres.lct	Low cloud top pressure	Pa
Pres.mcb	Middle cloud base @ pressure	Pa
Pres.mct	Middle cloud top pressure	Pa
Pres.sfc.gauss	Surface pressure	Pa
Rhum	Relative humidity @ pressure	%
Ugwd.sfc.gauss	U wind @ sfc	m/s
Uwind.10m.gauss	U wind @ 10m	m/s
Uwnd	U wind @ pressure	m/s
vgwd.sfc.guass	V wind @ sfc	m/s
vwind.10m.gauss	V wind @ 10m	m/s
vwnd	V wind @ pressure	m/s

As of now, the parameters that will be used are:

- Precipitation Rate at the surface
- Relative Humidity
- Air temperature at the surface
- Surface pressure

To get the precipitation rates at the time and place of interest:

- Filename = 'prate.sfc.gauss.1999.nc'
- Parameter = ‘prate’

- Latitude = 8.7
    - Because on August 6, AMPR collected data from 7.99 – 9.36 degrees, and halfway into that range is 8.675
- Longitude range = [166.5;169]
    - Because on August 6, AMPR collected data from 167.17 – 168.77 degrees, and halfway into that range is 167.97
- Time range = [1749600;1749606]
    - Because on August 6, AMPR collected data from 0320 to 0512
    - NOAA timestamps their data with the number of hours that have passes since January 1, 1800.
    - Using this website's calculator: https://www.convertunits.com/dates/from/Jan+1,+1800/to/Aug+6,+1999 it was determined that August 6, at 0000 was 1749600 hours from Jan. 1, 1800.
    - Therefore AMPR collected data from 1749603 to 1749606, and halfway into that range is 1749604.5

From there, put it all in the MATLAB command window as:
test_reader('prate.sfc.gauss.1999.nc', 'prate', 8.675,167.97,1749604.5)
This yields: -2.3283e-10, which will be rounded to **0**

To Get The Surface Pressure Value Of Interest:

- Filename = 'pres.sfc.gauss.1999.nc'
- Parameter = 'pres'
- All other input parameters are the same

From there, we put it all in the command window as:
test_reader('pres.sfc.gauss.1999.nc', 'pres', 8.675,167.97,1749604.5)

This yields: 101110 Pa. which converts to **1011.1 mb**

To get the Relative Humidity values of interest:

- Filename = 'rhum.1999.nc'
- Parameter = 'rhum'
- The other inputs are the same

From there, we put it all in the command window as:
test_reader('rhum.1999.nc', 'rhum', 8.675,167.97,1749604.5)

This yields: **[82;85;86;71;40;24;7;0;0;0;43;68;14;4;1;1;0] % Humidity**

To Get The Air Temperature Value At 2m Of Interest:

- Filename = 'air.2m.gauss.1999.nc'
- Parameter = ‘air’
- The other inputs are the same

From there, we put it all in the command window as:
test_reader('air.2m.gauss.1999.nc', 'air',8.675,167.97,1749604.5)
This yields: **301.28 K which is 82.634 F**

Determining the Presence Of Clouds And Rain:

To determine the presence of potential clouds and rain, one utilizes LEEDR’s weather cube capabilities. This is done by running a modified runFullHydra.m code. This code has been modified to accept .nc data files, and reads the 1999 climatological data.

To do this, open runFullHydra.m and type in the command window:

runFullHydra('OutputFolder','1999 Climatological Data\1999_NetCDF','kwajalein','Friz')

The command window will then prompt for:

- How many profiles to make
    - Weather cubes are large, and computationally intensive. For this project, the area AMPR covered while collecting data is small enough to be encapsulated by a single profile
    - Enter **1** for this example
- What year the data is in
    - Enter as **1999** for this example
- What month the data is in
    - Enter as **08** for this example
- What day the data is in
    - Enter as **06** for this example
- What cycle the data is in (meaning 0000-0600, 0600-1200, 1200-1800, or 1800-2400)
    - Enter in 0, 600, 1200, or 1800
    - For this example, AMPR collected data on Aug. 6 from 0320 to 0512, so the cycle is **0**
- What time is the data of interest
    - Enter in the number of hours since Jan, 1, 1800.
    - For this example, as calculated earlier, it is: **1749604.5**

Once the data meshes are created, one can plot them using the mess_plotter.m script.

One can review the Weather Cube User Guide to understand what each mesh is.

Plotting the wx mesh:

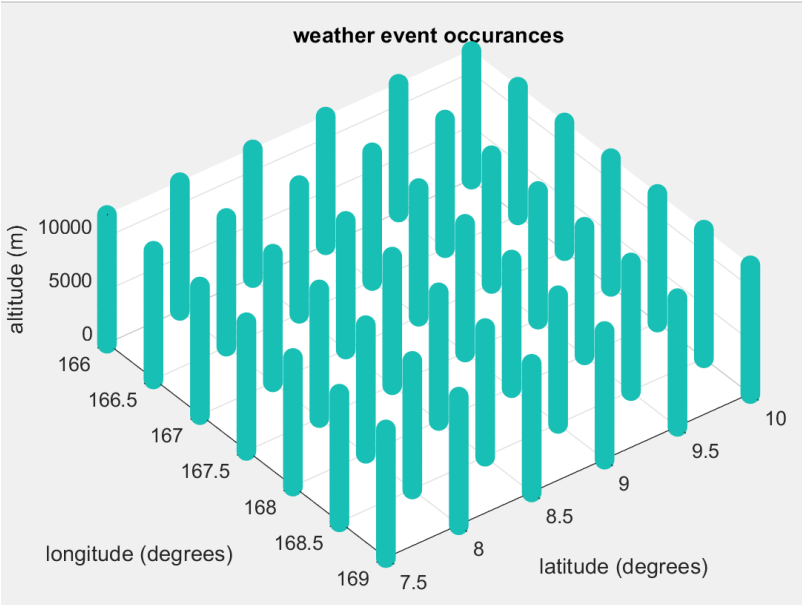

Knowing the wx mesh is a mesh of Boolean values, where a 1 indicates the presence of a weather event, this plot indicates there is not a single weather event in this profile based on the data provided. As a result, the LEEDR simulation below will **have clear weather under the clouds and rain tab.**

Had a weather event been indicated, one would then consult the Weather_Algorithm pdf, and study other meshes to determine what kind of weather event each instance is.

Starting the LEEDR Simulation:

Fill in the inputs on the various tabs:

Location:
ExPERT's Kwajalin Location was used at
Latitude: 8.73
Longitude: 167.73
This is within AMPR's measurement range, so we select that.

Atmosphere:

- Atmosphere
    - Summer,

    - 0300-0600 time of day, in agreement with AMPR's time of measurement
    - RH set to XX, in agreement with NOAA measurements.
- Aerosols:
    - Ignore
- Settings:
    - Use correlated-K
    - 1000 layers
- Molecular:
    - Ignore
- Wind:
    - Ocean
- Turbulence
    - Ignore

Aerosols:

- Ignore whole tab

Clouds and Rain

- There was no rain, so no clouds either

Laser/Geometry:

- Layers
    - Path resolution: 1000
- Wavelength
    - User Wavelength (m): 0.02801 (corresponds to 10.7 GHz, in agreement with AMPR)
- Path Type:
    - Slant Path
- Slant Path:
    - Platform Altitude (m): 0
    - Target Altitude (m): 13000
        - AMPR flew at an average altitude of 13000 ft.
    - Path Length (m): 13000
- Ground Level
    - Pressure (mb): 1011.1
    - Air Temperature (degrees F): 82.634
    - Dew Point: ignore
    - Relative Humidity (%): Ignore
    - Sea temperature (degrees F): Ignore
    - MAMSL: Ignore
    - Wind Speed (m/s): Ignore

Once all the above is entered in, create the profile, to get:

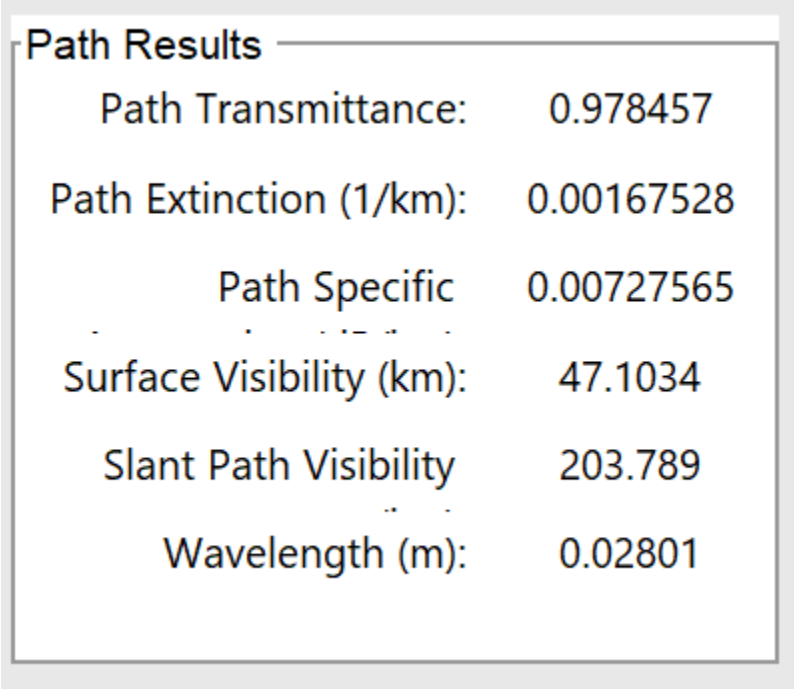

Now open the Path Radiance Section:

Path Radiance

- **Inputs**
  - Wavelength
    - Set wavelength range from 0.04-0.02
    - molecular points: 100
    - Aerosol points: 10
    - Use multi scatter
    - Use correlated K
  - Path
    - Altitude: 13000
    - Zenith: 180
    - Azimuth: 0
    - Resolution: 200
  - Surface
    - Check surface type box, set to Ocean_Water
    - User Emissivity: 0.4
    - User Albedo: 0.6

        - Temperature: 300
    - Path Type
        - Slant Path
    - Target Params
        - Ignore
    - Date and Time (UTC)
        - August 6, hour 6, minute 0, second 0
    - User Sun/Moon Angles
        - Ignore

Then press the calculate button

- Path Radiance:
    - Select Total Thermal
    - Using the printable plot one can get the figure below:

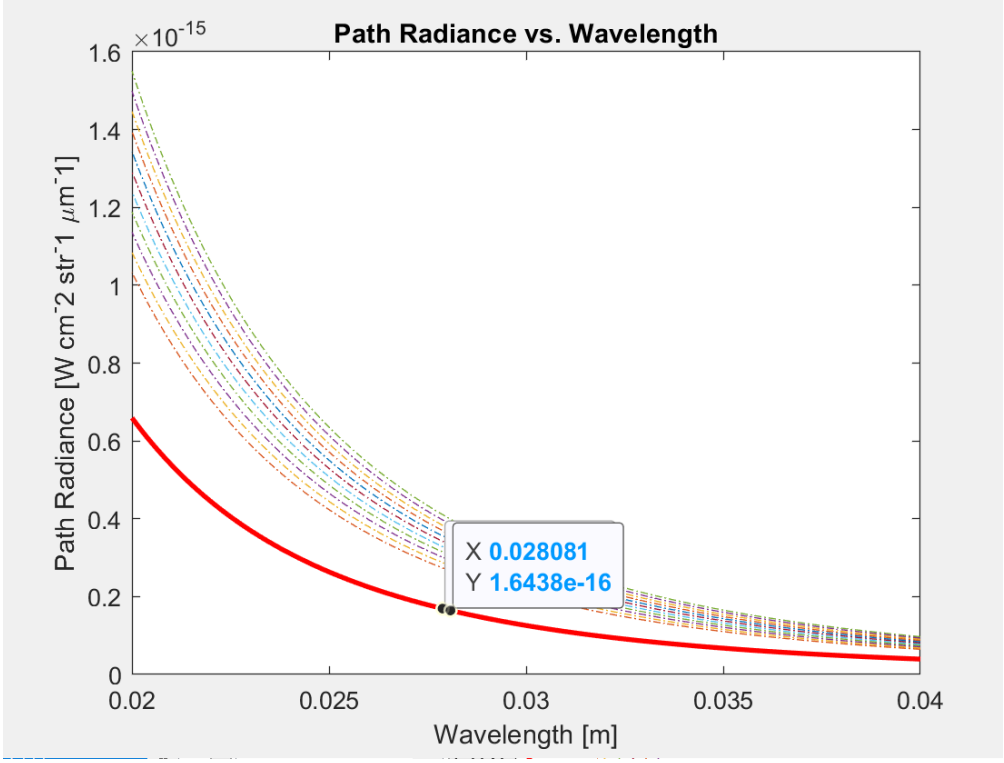

From here, use the inverse planck function to calculate brightness temperature. There is a calculator on this website for it: https://ncc.nesdis.noaa.gov/data/planck.html

Convert LEEDR's calculated values into units compatible with the calculator like so:

- Path Radiance: multiply by 10^4 to convert from W*(cm^-2)*(str^-1)*(um^-1) to W*(m^-2)*(str^-1)*(um^-1)

- So 1.6438e-16 becomes 1.6438e-12
- Center Wavelength: multiply by 10^6 to convert from m to um.
  - So 0.028 m becomes 28000 um

Which gives the following result in the figure below:

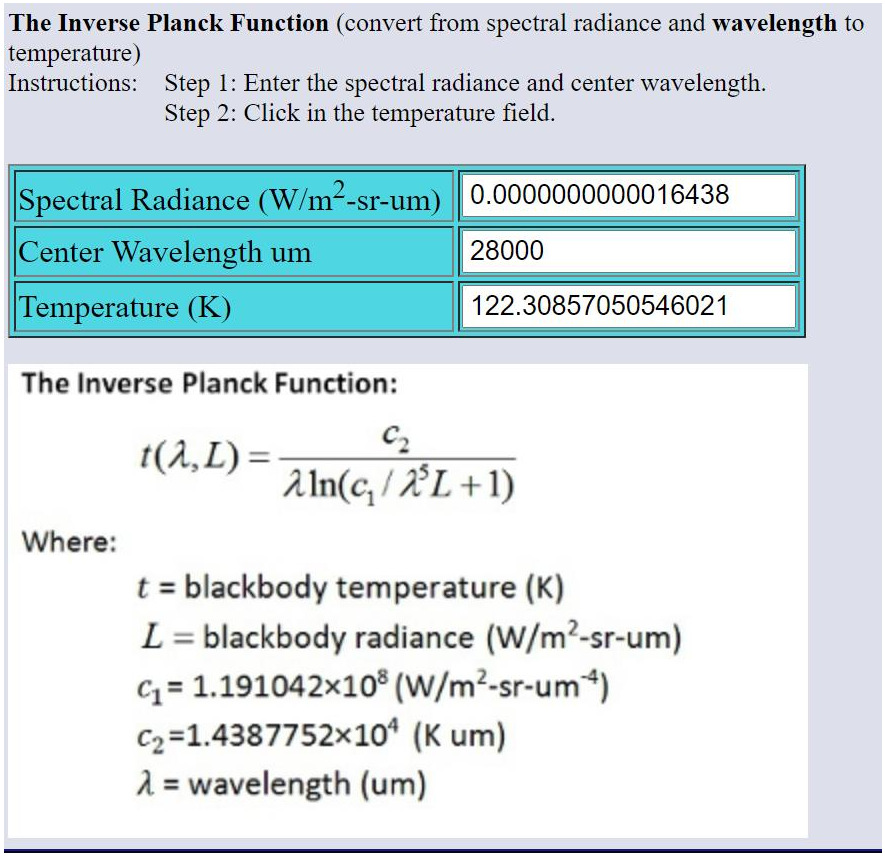

The Inverse Planck Function (convert from spectral radiance and **wavelength** to temperature)
Instructions: Step 1: Enter the spectral radiance and center wavelength.
Step 2: Click in the temperature field.

Spectral Radiance (W/m^2-sr-um)	0.0000000000016438
Center Wavelength um	28000
Temperature (K)	122.30857050546021

The Inverse Planck Function:

$$t(\lambda, L) = \frac{c_2}{\lambda \ln(c_1 / \lambda^5 L + 1)}$$

Where:

t = blackbody temperature (K)
L = blackbody radiance (W/m^2-sr-um)
c_1 = 1.191042×10^8 (W/m^2-sr-um^{-4})
c_2 = 1.4387752×10^4 (K um)
λ = wavelength (um)

The last measured nadir value on August 6, 1999 by AMPR was at 0522, with a brightness temperature of 135.42 K. From this, one can see that LEEDR calculations only differ from measured values by ~13 K.

ADDITIONAL TESTING:

By altering the clouds and rain settings in LEEDR, one can increase the brightness temperatures to more closely match AMPR measured values. Although the usage of these clouds is guesswork, results are below.

The entire profile is kept the same as above, aside from cloud and rain settings, which will be labeled in the results below:

Note: Last recorded AMPR brightness temperature on Aug 6, was 135.42 K, which correlates to a spectral radiance of **1.82037e-16** W*(cm^-2)*(str^-1)*(um^-1)

Trial 1:

Change: Cumulus Maritime from 12000-14000 ft:

Results:

Path radiance at wavelength 0.028081 m: 1.6703e-16

Trial 2:

Change: Cumulus Maritime from 12000-14000 ft, moderate rain, 13000-0 ft

Results:

Path radiance at wavelength 0.028081 m: 2.5057e-16

Trial 3:

Change: Cumulus Maritime from 12000-14000 ft, light rain, 13000-0 ft

Results:

Path radiance at wavelength 0.028081 m: 2.0519e-16

Trial 4:

Change: Cumulus Maritime from 12000-14000 ft, very light rain, 13000-0 ft

Results:

Path radiance at wavelength 0.028081 m: 1.818e-16

Trial 5:

Change: Stratus Maritime from 12000-14000 ft, very light rain, 13000-0 ft

Results:

Path radiance at wavelength 0.028081 m: 1.8094e-16

Trial 6:

Change: Stratus Maritime from 11000-15000 ft, very light rain, 13000-0 ft

Results:

Path radiance at wavelength 0.028081 m: 1.8294e-16

Trial 7:

Change: Stratus Maritime from 11500-14000 ft, very light rain, 13000-0 ft

Results:

Path radiance at wavelength 0.028081 m: 1.8194e-16

Trial 8:

Change: Stratus Maritime from 11100-14000 ft, very light rain, 13000-0 ft

Results:

Path radiance at wavelength 0.028081 m: 1.8273e-16

Trial 9:

Change: Stratus Maritime from 11300-14000 ft, very light rain, 13000-0 ft

Results:

Path radiance at wavelength 0.028081 m: 1.8234e-16

Trial 10:

Change: Stratus Maritime from 11400-14000 ft, very light rain, 13000-0 ft

Results:

Path radiance at wavelength 0.028081 m: 1.8213e-16

This calculates to 135.48 **which is only 0.06 K off from the measured value.**

Appendix C

Raw data used to create Figures 14 and 15

Date	Time in hours from jan. 1, 1800	Measured TB (K)	Sample #	Altitude (m)	Recorded Rain Rate (mm/Hr)	Simulated TB (K) (no weather)	Simulated TB (K) (with weather)	Cloud Settings	Rain Settings	
08/03/1999	1749534	129.77	5767	10773	0.12564	122.4	129.63	cumulus maritime, 1000-3000m	5 mm/hr rain, 2750-0m	
08/09/1999	1749696	138.9	3674	12573	0	122.4	138.9	cumulus maritime, 1000-3000m	12.5 mm/hr rain, 2000-0m	
08/11-12/1999	1749744	176.85	5323	11596	0	122.37	176.57	cumulus maritime, 1000-3000m	35 mm/hr rain, 2100-0m	
08/14/1999	1749792	128.36	1687	11932	0	122.4	128.12	cumulus maritime, 1000-3000m	5 mm/hr rain, 2000-0m	
08/25/1999	1750062	121.07	4909	12549	0	122.3	122.3	none	none	no changes were made to this one
08/28-29/1999	1750152	122.27	2153	11296	0	122.36	122.36	none	none	no changes were made to this one

Results using METAR data for weather predictions

Date	Time in hours from jan. 1, 1800	Measured TB (K)	Sample #	Altitude (m)	Recorded Rain Rate (mm/Hr)	Simulated TB (K) (no weather)	Simulated TB (K) (with weather)	Cloud Settings	Rain Settings	
08/03/1999	1749534	129.77	5767	10773	0.12564	122.4	129.67	Stratus maritime 1500-3500 m, Cumulus Maritime 3500-6900 m, Cirrus (-25 C) 7000-9000 m	none	
08/09/1999	1749696	138.9	3674	12573	0	122.4	138.7	Cumulus Maritime 457-9500 m, Stratus Maritime 500-2500 m, Cirrus (-50 C) 8000-10500 m	none	
08/11-12/1999	1749744	176.85	5323	11596	0	122.37	176.3	Cumulus Maritime 457-11000 m, Cirrus (-25 C) 8000-11000	14 mm/Hr rain 0-5000 m	
08/14/1999	1749792	128.36	1687	11932	0	122.4	128.2	Cumulus Maritime 3000-5750 m, Cirrus (-25 C) 7000-9000 m, Stratus Maritime 1000-3000 m	none	
08/25/1999	1750062	121.07	4909	12549	0	122.3	122.3	none	none	no changes were made to this one
08/28-29/1999	1750152	122.27	2153	11296	0	122.36	122.36	none	none	no changes were made to this one

Appendix D

Rain Rate Curve Development Process:

This document outlines how the rain rate vs. brightness temperature curve presented in the paper: "Critical Assessment of Microphysical Assumptions within TRMM Radiometer Rain
Profile Algorithm Using Satellite, Aircraft, and Surface Datasets from KWAJEX" was

replicated within LEEDR.

Starting the LEEDR Simulation:

Fill in the inputs on the various tabs:

Location:
Select ExPERT's Kwajalin Location:
Latitude: 8.73
Longitude: 167.73

Atmosphere:

- Atmosphere
    - Summer,
    - 15-18 time of day, to ensure the sun does not influence results
    - RH Bin: 99%
- Aerosols:
    - Ignore
- Settings:
    - Use correlated-K
    - Check boundary layer box.
        - Set box value to 4000
    - 1000 layers
- Molecular:
    - Ignore
- Wind:
    - Ocean
- Turbulence
    - Ignore

Aerosols:

- Ignore whole tab

Clouds and Rain

- Custom Weather from 500 – 6000 m
    - Type: Cumulus Maritime
    - Adjust “A” term with rain rate as shown in the associated rain rate vs. brightness temperature excel file.
- Custom Weather from 0 – 4000 m
    - Type: Heavy Rain
    - Adjust “Max” to 2000 um.
    - Adjust “Rain” as shown in the associated excel file.
- Cumulus Maritime from 6000 – 10000 m

Laser/Geometry:

- Layers
    - Path resolution: 1000
- Wavelength
    - User Wavelength (m): 0.03 (corresponds to 10 GHz)
- Path Type:
    - Slant Path
- Slant Path:
    - Platform Altitude (m): 0
    - Target Altitude (m): 100000 m
        - Arbitrarily Chosen Satellite Altitude
    - Path Length (m): 100000 m
- Ground Level
    - Pressure (mb): 1012
    - Air Temperature (degrees F): 83
    - Dew Point: 75
    - Relative Humidity (%): Ignore
    - Sea temperature (degrees F): Ignore
    - MAMSL: Ignore
    - Wind Speed (m/s): Ignore

Once all the above is entered in, create the profile.

Next open the Path Radiance Section

Path Radiance

- **Inputs**
    - Wavelength
        - Set wavelength range from 0.04-0.02
        - molecular points: 100
        - Aerosol points: 10

        - Use multi scatter
        - Use correlated K
    - Path
        - Altitude: 100000
        - Zenith: 180
        - Azimuth: 0
        - Resolution: 200
    - Surface
        - Check surface type box, set to Ocean_Water
        - User Emissivity: 0.4
        - User Albedo: 0.6
        - Temperature: 300
    - Path Type
        - Slant Path
    - Target Params
        - Ignore
    - Date and Time (UTC)
        - August 11, hour 18, minute 0, second 0
    - User Sun/Moon Angles
        - Ignore

Then press the calculate button

- Path Radiance:
    - Select Total Thermal
    - Using the printable plot to determine the values

The values generated and the cloud and rain parameters each result was set to can be found in the associated excel document: Rain Rate Curve Data, on sheet 4.

The following plots were generated from the results:

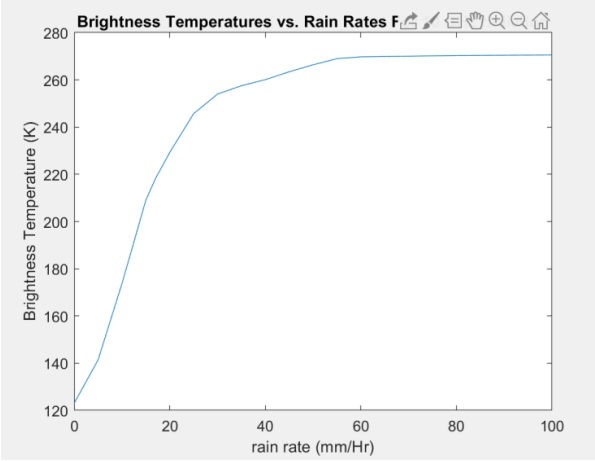

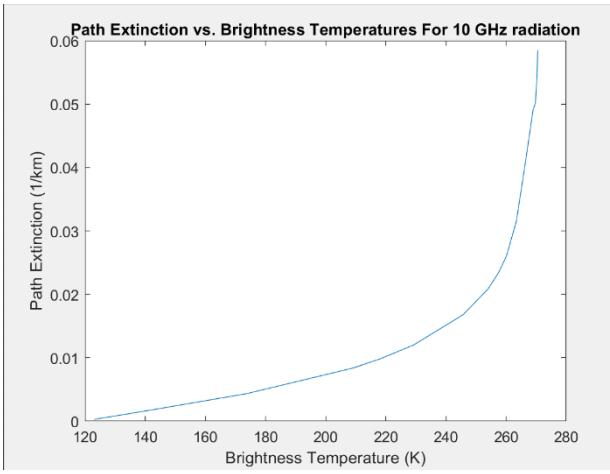

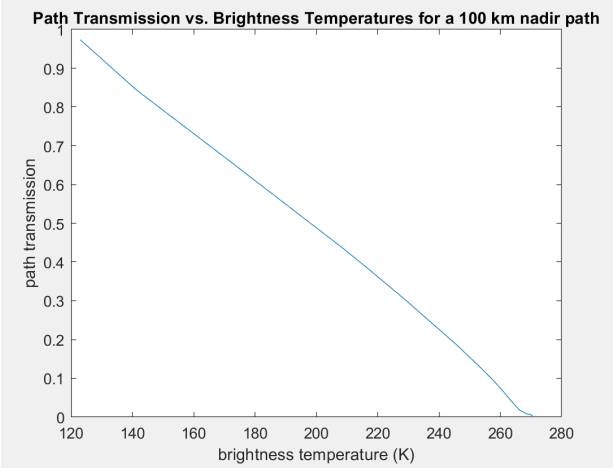

The raw data is below.

Cloud Settings		"A" value for custom cloud	Rain altitude	Rain Rate in mm/Hr	Rain radii in microns	path radiance (in e-16 path rad	brightness temperature (K)	Path Transmittance	Path Extinction (1/km)	Path Specific Attenuation (dB/km)
none	none	N/A	N/A	0	N/A	1.255	123.03	0.973142	0.00027225	0.00118237
Maritime c	Custom Ma	0.00001	0-4000m	5	50-2000	1.4427	141.4	0.843439	0.00170268	0.00739464
		0.00023		10		1.7731	173.73	0.648349	0.00433326	0.0188191
		0.00065		15		2.1344	209.08	0.43305	0.00836902	0.0363461
		0.00079		17		2.2272	218.16	0.374415	0.00982391	0.0426647
		0.001		20		2.341	229.29	0.300714	0.012016	0.0521846
		0.0015		25		2.5088	245.71	0.1867	0.0167825	0.0728856
		0.0019		30		2.5933	253.98	0.124583	0.0208278	0.0904539
		0.0021		35		2.6294	257.52	0.0962033	0.0234129	0.101681
		0.0023		40		2.6558	260.1	0.0743044	0.0259959	0.112898
		0.0029		45		2.6898	263.42	0.042857	0.0314989	0.136798
		0.004		50		2.7201	266.39	0.0171608	0.0406513	0.176546
		0.005		55		2.7465	268.976	0.00739908	0.049064	0.213082
		0.005		60		2.7544	269.75	0.00663475	0.0501543	0.217817
		0.005		80		2.7601	270.308	0.00433289	0.0544152	0.236322
		0.005		100		2.7623	270.523	0.00287655	0.0585116	0.254133

Bibliography

1. A. B. Badiru, C. B. Barlow, J. E. Schmidt, J. L. Burley, B. J. Elmore, S. T. Fiorino, K. J. Keefer, and N. R. Van Zandt, "4D Weather Cubes And Defense Applications," in *Defense Innovation Handbook: Guidelines, Strategies, and Techniques*, Boca Raton ; London ; New York: CRC Press, 2019, pp. 257–279.

2. B. A. Shelters, "Satellite Communications in the V and W Band: Tropospheric Effects," thesis, AFIT, Dayton, 2018.

3. C. Cao and X. Shao, "Planck Function Converter," *Planck Function*. [Online]. Available: https://ncc.nesdis.noaa.gov/data/planck.html. [Accessed: 5-Nov-2020].

4. Center for Directed Energy, "LEEDR Equations And Principles (LEAP)." Air Force Institute of Technology, Dayton, Jul-2020.

5. ConvertUnits.com, "Measurement Unit Converter," *convert units*. [Online]. Available: https://www.convertunits.com/. [Accessed: 5-Nov-2020].

6. D. A. Mahmood and K. J. Al-Jumaily, "Estimation of Dual Polarization Weather Radar Variables," *Al-Mustansiriyah Journal of Science*, vol. 28, no. 2, pp. 1–6, 2017.

7. D. Puent, "INTEGRATION OF ADAPTIVE OPTICS INTO HIGH ENERGY LASER MODELING AND SIMULATION," thesis, Naval Postgraduate School, Monterey, 2017.

8. E. P. Magee M. R. Whiteley and A. M. Ngwele. Scaling for High Energy Laser and Relay Engagement (SHaRE) User Guide. MZA Associates, Dayton OH, 2011.

9. Grant W. Petty. A First Course in Atmospheric Radiation. Sundog Publishing, Madison WI, 2004.

10. Hersbach, H., Bell, B., Berrisford, P., Biavati, G., Horányi, A., Muñoz Sabater, J., Nicolas, J., Peubey, C., Radu, R., Rozum, I., Schepers, D., Simmons, A., Soci, C., Dee, D., Thépaut, "ERA5 hourly data on pressure levels from 1979 to present" *Copernicus Climate Change Service (C3S) Climate Data Store (CDS)*. [Accessed on 09-Dec-2020], 10.24381/cds.bd0915c6

11. Jaclyn E. Schmidt AFIT/CDE. Weather Cube User Guide, Dayton, 2020.

12. J. B. Roberts, “AMPR Brightness Temperature (TB) KWAJEX,” *HyDRO Search*. [Online]. Available: https://doi.org/10.5067/KWAJEX/AMPR/DATA101. [Accessed: 28-Dec-2020].

13. J. M. Wallace and P. V. Hobbs, *Atmospheric science: an introductory survey*. Amsterdam: Elsevier Acad. Press, 2011.

14. K. L. S. Gunn and T. W. R. East. The Microwave Properties of Precipitation Particles. Quarterly Journal of the Royal Meteorological Society, 80(346):522-545, 1954.

15. M. Hess, P. Koepke, and I. Schult, “Optical Properties of Aerosols and Clouds: The Software Package OPAC.” Bulletin of the American Meteorology Society, 29-Jan-1998.

16. National Oceanic and Atmospheric Association and National Centers For Environmental Information, “NCEP/DOE Global Reanalysis (Reanalysis-II) .” .

17. Nicholas C. Currie. Millimeter-Wave Radar Clutter. Artech House, Boston, 1992.

18. P. Jaffe, K. Borders, C. Browne, C. DePuma, L. Longbottom, H. Nisar, and V. Simlot, “Opportunities and Challenges for Space Solar for Remote Installations.” Office of the Under Secretary of Defense for Research and Engineering (OUSD(R&E)), The Pentagon, 21-Oct-2019.

19. Plymouth State Weather Center. https://vortex.plymouth.edu/myo/sfc/statlog-a.html [Accessed: 7-Dec-2020].

20. R. D. Cook, “Capturing Atmospheric Effects on 3-D Millimeter Wave Radar Propagation Patterns,” thesis, AFIT, Dayton, 2016.

21. R. F. Adler, H.-Y. M. Yeh, N. Prasad, W.-K. Tao, and J. Simpson, “Microwave Simulations of a Tropical Rainfall System with a Three-Dimensional Cloud Model,” *Journal of Applied Meteorology*, vol. 30, no. 7, pp. 924–953, 1991.

22. RK Crane and DW Blood. Handbook for the Estimation of Microwave Propagation Effects: Link Calculations for Earth-Space Paths (Path Loss and Noise Estimation). NASA STI/Recon Technical Report N, 82:12301, 1979.

23. S. T. Fiorino and E. A. Smith, “Critical Assessment of Microphysical Assumptions within TRMM Radiometer Rain Profile Algorithm Using Satellite, Aircraft, and Surface Datasets from KWAJEX,” *Journal of Applied Meteorology and Climatology*, vol. 45, no. 5, pp. 754–786, 2006.

24. Steven T Fiorino, Richard J Bartell, Matthew J Krizo, Gregory L Caylor, Kenneth

P Moore, Thomas R Harris, and Salvatore J Cusumano. A First Principles Atmospheric Propagation & Characterization Tool: the Laser Environmental Effects Definition and Reference (LEEDR). In Lasers and Applications in Science and Engineering, pages 68780B-68780B. International Society for Optics and Photonics, 2008.

25. S. T. Fiorino, R. M. Randall, M. F. Via, and J. L. Burley, "Validation of a UV-to-RF High-Spectral-Resolution Atmospheric Boundary Layer Characterization Tool," *Journal of Applied Meteorology and Climatology*, vol. 53, no. 1, pp. 136–156, 2014.

26. S. V. Hum, "Atmospheric Effects," in *ECE 422*.

27. Warren J Wiscombe. Improved Mie Scattering Algorithms. Applied optics, 19(9):1505-1509, 1980.

28. Y. H. Lee and Y. S. Meng, "Key Considerations in the Modeling of Tropical Maritime Microwave Attenuations," *International Journal of Antennas and Propagation*, vol. 2015, pp. 1–7, Mar. 2015.

REPORT DOCUMENTATION PAGE

Form Approved
OMB No. 074-0188

1. REPORT DATE *(DD-MM-YYYY)*	**2. REPORT TYPE**	**3. DATES COVERED** *(From – To)*
18-02-2021	Master's Thesis	June 2020 – March 2021

TITLE AND SUBTITLE

AN ANALYSIS OF X-BAND RADIATION FOR SPACE-BASED WIRELESS POWER TRANSMISSION

5a. CONTRACT NUMBER

5b. GRANT NUMBER

5c. PROGRAM ELEMENT NUMBER

6. AUTHOR(S)

Friz, Noah W., 1st Lt, USAF

5d. PROJECT NUMBER

5e. TASK NUMBER

5f. WORK UNIT NUMBER

7. PERFORMING ORGANIZATION NAMES(S) AND ADDRESS(S)
Air Force Institute of Technology
Graduate School of Engineering and Management (AFIT/ENG)
2950 Hobson Way, Building 640
WPAFB OH 45433-8865

8. PERFORMING ORGANIZATION REPORT NUMBER

AFIT-ENG-MS-15-M-000

9. SPONSORING/MONITORING AGENCY NAME(S) AND ADDRESS(ES)
Air Force Research Laboratory
AFRL/RXSC, Bldg651 Rm 59 2179 12th Street
937-904-5046 (DSN 674), brian.hans@us.af.mil
ATTN: POC

10. SPONSOR/MONITOR'S ACRONYM(S)

AFRL/RXSC

11. SPONSOR/MONITOR'S REPORT NUMBER(S)

12. DISTRIBUTION/AVAILABILITY STATEMENT
DISTRUBTION STATEMENT A. APPROVED FOR PUBLIC RELEASE; DISTRIBUTION UNLIMITED.

13. SUPPLEMENTARY NOTES
This material is declared a work of the U.S. Government and is not subject to copyright protection in the United States.

14. ABSTRACT

The USAF is interested in developing a solar powered satellite power beaming system using X-Band radiation. To determine the expected level of transmission efficiency of the system, an atmospheric characterization and radiative transfer modeling system called LEEDR was employed. A study was conducted to validate LEEDR's performance while working with microwave frequencies by replicating brightness temperatures measured by a 10.7 GHz radiometer above the Pacific Ocean in 1999. The results were inconclusive. Brightness temperature vs. rain rate curves developed within other studies for X-Band radiation curves could be replicated within LEEDR, and therefore the associated path transmission and extinction values. These values can serve as a lookup table between brightness temperatures and attenuation for 10 GHz radiation, which provide useful metrics for determining expected transmission efficiencies.

15. SUBJECT TERMS
Wireless Power, Power Beaming, Microwave Radiation, X-Band

16. SECURITY CLASSIFICATION OF:			**17. LIMITATION OF ABSTRACT**	**18. NUMBER OF PAGES**	**19a. NAME OF RESPONSIBLE PERSON**
a. REPORT	**b. ABSTRACT**	**c. THIS PAGE**			Dr. Andrew Terzuoli, AFIT/ENG
U	**U**	**U**	**UU**	79	**19b. TELEPHONE NUMBER** *(Include area code)* (937) 255-6565, ext xxxx (NOT DSN) (terzuoli@afit.edu)

Standard Form 298 (Rev. 8-98)
Prescribed by ANSI Std. Z39-18